LBL-27258
Preprint

Lawrence Berkeley Laboratory
UNIVERSITY OF CALIFORNIA

Materials & Chemical Sciences Division

National Center for Electron Microscopy

Submitted to Philosophical Magazine

On the Formation of Twinned Precipitates in Al-Ge Alloys

J. Douin, U. Dahmen, and K.H. Westmacott

November 1989

Prepared for the U.S. Department of Energy under Contract Number DE-AC03-76SF00098.

DISCLAIMER

Submitted to Phil. Mag.

On the Formation of Twinned Precipitates in Al-Ge Alloys

By J. DOUIN* , U. DAHMEN and K.H. WESTMACOTT

National Center for Electron Microscopy, Materials and Molecular Research Division, University of California, Lawrence Berkeley Laboratory,

Berkeley, California 94720, U.S.A.

ABSTRACT

High resolution microscopy has been used systematically to obtain a detailed understanding of the morphologies and substructures of Ge needle or lath precipitates in an Al-Ge alloy. We show that the many orientation relationships observed in twinned <100> and <110> needles can be related to only three basic lattice correspondences. The feature common to <100> and <110> needles is the arrangement of five cozonal twin segments whose relative degree of development determines the cross section morphology. Proposed growth mechanisms based on multiple twinning can account for the formation of all the different observed precipitate morphologies and defect substructures. The central role of twinning and the critical need for vacancies during nucleation are discussed in terms of possible models for nuclei that maximize the number of Ge-Ge bonds through twinning and thus minimize the need for vacancies.

---

* Present address : Institut de génie atomique, Ecole Polytechnique Fédérale de Lausanne, Département de physique, PHB- Ecublens, CH - 1015 Lausanne, Switzerland

§ 1. INTRODUCTION

Aluminum-germanium and aluminum-silicon alloys are metallurgically simple. Both form eutectics and have limited and strongly temperature dependent Al-rich terminal solid solubilities which gives rise to classical age-hardening behavior. In both systems an appropriate quench/age treatment results in direct precipitation of the equilibrium pure Ge or Si phase without intermediate phase formation. In contrast to their simple phase diagrams, however, the morphology of the precipitate structures as determined by transmission electron microscopy studies is surprisingly complex (Saulnier 1961, Köster 1969, 1971, Gouthama, Subbanna and Kishore 1985, Gouthama and Kishore 1987, Hugo and Muddle 1986, Westmacott and Dahmen 1986, 1987). Al-Si alloys form plate, needle and lath precipitates on various habits (Saulnier 1961, Westmacott and Dahmen 1985) while in Al-Ge alloys similar morphologies but sometimes different habits have been reported (Köster 1969, 1971, Hugo and Muddle 1986, 1989). Several different orientation relationships were determined in most of the investigations but the results were generally consistent. A common feature of the observations was the occurrence of twinning in the precipitate particles (Köster, 1969, Gouthama et al. 1985, 1987, Dahmen and Westmacott 1986).

In many respects Al-Ge and Al-Si are ideal model systems for studying precipitation, and some aspects, particularly nucleation, have been investigated in detail (Rosenbaum and Turnbull 1958, 1959, Lorimer and Nicholson 1969, Russell 1969, Ozawa and Kimura 1970, Beller 1972, Westmacott and Dahmen 1987). This work has verified the indispensable role of vacancies in the nucleation and growth processes. However, a detailed understanding of precipitation in these systems is hindered by the formidable obstacle of explaining how at the atomic scale the relatively open Ge and Si diamond-cubic structures can form and grow in the close-packed Al face-centered cubic matrix. In the present contribution a systematic atomic resolution microscopy study of

needle- and lath-shaped precipitate morphologies and substructure in an Al-Ge alloy was conducted to elucidate the role of twinning in precipitate nucleation and growth.

§ 2. ORIENTATION RELATIONSHIPS

Precipitation in Al-Ge, and also Al-Si, is noted for the variety of different orientation relationships (OR) that is observed, and a summary has been compiled in Table 1. Although orientation relationships are uniquely described in terms of a pair of parallel planes and a pair of parallel directions in that plane, three orthogonal pairs of parallel directions are given in Table 1 for completeness. Since both crystals are cubic, directions and plane normals are identical, and the usual brackets indicating planes or directions have been omitted. For clarity, specific indices (e.g. $1\bar{1}1$ rather than general e.g.111) have been used to show that the three pairs of indices used to describe each orientation relationship form an orthogonal set. Any such orthogonal set can of course be replaced with a crystallographically equivalent one.

One of the predominant precipitate morphologies in Al-Ge is the needle or rod precipitate which grows with a large aspect ratio. High resolution TEM observations (Dahmen and Westmacott 1986b) have shown that these precipitates have a $<110>_{Ge}$ direction accurately parallel to $<100>_{Al}$ along the needle axis and that they invariably display internal twinning.

2.1. *<100> Precipitates*

A simple way to illustrate systematically the possible OR's for <100> needles is shown in fig. 1 where four different orientation relationships are seen as the relative rotation of one polygon within another. The truncated square represents the symmetry of the Al matrix in <100> projection while the inscribed truncated rectangle represents the symmetry of the Ge precipitate in <110> projection. Thus this figure illustrates those precipitates that have a fourfold 100 symmetry axis in Al accurately parallel to a twofold 110 symmetry axis in Ge, an alignment that was in fact found in

most of the particles examined. Note that due to this alignment ($100_{Al} \parallel 110_{Ge}$) the two crystals share a common 2/m symmetry along the axis of these needles and the orientation relationship is at a symmetry-dictated extremum (Cahn and Kalonji 1981).

One may now imagine the precipitate crystal rotating freely inside the matrix around this common axis which it can do without destroying the common 2/m symmetry in this zone. At some special angles of rotation, further symmetry elements will come into coincidence. Four such special orientation relationships, all based on the common twofold axis, are seen in fig. 1. Figure 1(a) shows the alignment with the highest degree of symmetry. From here the other orientation relationships, shown in figs. 1 (b)-(d), can be reached by a rotation of 45°, 35.27° and 9.74°, respectively. The latter two have $1\bar{1}1$ of Ge parallel to either 001 or 011 of the Al. Note that these are alignments of symmetry axes with no common symmetry elements and do not therefore represent symmetry-dictated extrema.

A more accurate way of illustrating the orientation relationships in fig. 1 is the stereographic representation in fig. 2. The symmetry elements are indicated by conventional symbols : rotation axes by two-, three-, and fourfold symbols and vertical mirror planes by solid lines. The matrix orientation is fixed and the precipitate orientation, given by the inscribed circle, is variable. It is now easy to see the symmetry of the orientation relationship for each case. Figure 2(a) displays tetragonal 4/mmm symmetry, fig. 2(b) orthorhombic 222 and figs. 2(c) and (d) exhibit only the monoclinic symmetry of the common rotation axis since the alignment of a triad with an evenfold axis does not lead to any shared symmetry elements. However, these orientation relationships do become special when twinning is taken into account.

2.2. *Twinning*

Due to the extensive twinning observed in Ge and Si precipitated not only from the bulk but also on alloy surfaces, and in pure materials during eutectic solidification, it is important to separate

precipitate orientations that are mutually related by internal twinning from those that are truly distinct from each other.

Internal twinning of a precipitate by reflection across a {111} plane leads to a new Ge orientation related to the primary Ge by a 70.53° rotation about a <110> direction in the twin plane. In the schematic representation of figs. 1 and 2 each of the rational orientation relationships could thus generate further orientation relationships with the same alignment of zone axes (common 2/m symmetry) by internal twinning. Primary twinning leads to a rotation of 70.53°, secondary twinning to an additional rotation of 70.53°, and so on. If twinning occurs on the other twin plane in the common zone it will add a rotation of -70.53°. Multiple twinning is most likely to occur on both twin planes, and the primary twins on each of the two twin systems will be related to each other by twice the rotation angle. Note, however, that the two primary twins obey different variants of the same orientation relationship with the matrix: they are related to each other by a mirror reflection across the common {001} planes in fig. 1(a).

Similarly, because a twin plane in the Ge is parallel to a mirror plane in the Al in figs. 1(c) and (d), primary twinning on that plane will only lead to a different variant of the same orientation relationship. Thus by twinning on a {111} plane that is parallel to a matrix mirror, a precipitate can maintain the same orientation relationship (albeit a different variant) with the matrix.

Starting from one of the special OR's in fig. 1 it is clear that none of the other special OR's can be obtained precisely by a small number of successive twinning operations. However, as shown in fig. 3, two successive twinning operations on the precipitate of fig. 1(a) bring it to within 3.67° (38.94 - 35.27) of that in fig. 1(c) and vice versa. Figures 1(b) and 1(d) are similarly related to each other. Furthermore, a double twinning operation brings the precipitate orientations of figs. 1(a) and 1(b) and figs. 1(c) and 1(d) to 6.06° (45-38.94) of each other. Thus if distortions up to this magnitude (6.06°) can be accommodated, all the OR's could be present in a multiply-twinned precipitate and could have originated from nuclei oriented in any one of the four possibilities shown in fig. 1.

2.3. *<110> Precipitates*

The second most common set of orientation relationships is found in needles or laths along <110> directions of the matrix. Again the <110> direction of the precipitate is accurately aligned with its counterpart in the matrix along the needle axis. Figure 4 illustrates the possible rational orientation relationships with this common zone axis. A stereographic representation similar to fig. 2 can be readily constructed, but is omitted here for brevity.

Note that in (a) all symmetry elements are shared: this is the cube-cube orientation relationship commonly observed for plate-shaped precipitates. The orientation relationships in (c) and (d) have the lowest composite symmetry because they have alignments of a threefold with a two- or fourfold axis. However, these are again important where multiple twinning is observed. Multiple twinning again brings some of the OR's close to each other. In this case, however, figs. 4(b) and (c) and figs. 4(a) and 4(d) are separated by 3.67° following a double twinning operation on either one of the pairs, but unlike the $<100>_{Al}$ needles no connection can be made between the two pairs. Thus allowing distortions up to 3.67° results in two basic orientations mutually related to two more OR's by double twinning.

Other rational orientation relationships could be constructed in this manner, but for the purpose of classifying and discussing the experimental observations, the two basic possibilities outlined above are sufficient. It is now possible to understand the connections between different orientation relationships in the multiply twinned particles so frequently observed in Al-Ge and Al-Si.

§ 3. EXPERIMENTAL

An alloy of nominal composition Al-1.10 at.% Ge was prepared from pure elements in the form of 0.1 mm foil. After ageing for a week at 550°C, 3 mm discs were quenched to -60°C in a solution of 75% HCl and 25% H_2O. Precipitation was ensured either by bulk or in-situ ageing for

approximately 4 h between 220°C and 260°C. Thin foils were prepared by jet-electropolishing using a solution of 85% methanol, 8% sulfuric acid, 5% lactic acid and 2% hydrofluoric acid between -26°C and -24°C and an operating current of 28 mA.

In-situ studies were carried out with the Kratos EM 1500 equipped with a Gatan double-tilt heating stage, and high resolution imaging of needle cross-sections was performed using the Berkeley JEOL ARM 1000 (operating at 800 kV).

§ 4. RESULTS

The overall precipitate morphology and distribution in quench/aged Al-Ge is shown in fig. 5. Approximately equal densities of plate and needle precipitates are observed in both bulk aged, fig. 5(a), and thin foil aged, fig. 5(b), specimens. In the thin foil experiments it has been possible to examine directly the influence of vacancy supersaturation on the type of precipitate nucleated (Westmacott and Dahmen 1987). It was observed that in thin regions of a foil where substantial loss of vacancies to the surfaces occurs needles are the predominant morphology nucleated, whereas near vacancy sources plate precipitates are favored. In thick regions of the foil equal distributions of needles and plates were found similar to the structures observed in bulk aged specimens. Very long coherent needles without Moiré contrast develop during thin foil aging, (see fig. 5(b)); this can be explained by elastic accommodation of the small mismatch between $<100>_{Al}$ and $<110>_{Ge}$ (~1.2%). When viewed end-on, the twinned substructure of the needles is evident even with diffraction contrast imaging. This is illustrated in fig. 5(c) for $<110>_{Al}$ needles with a <110> beam direction. Many examples of pentagonally-twinned precipitates with a characteristic dog-bone shape may be seen. Similar configurations, but with more symmetrical overall cross sectional shapes, are seen for end-on $<100>_{Al}$ needles in fig. 5(a).

Before presenting the results on the structure of twinned precipitates it is appropriate to review briefly related work on multiply-twinned-particles (MTP's) formed on substrates from the vapor phase (Ino, 1966, 1969; Heinemann, Jacamán, Yang and Poppa 1979; Marks 1984; Iijima 1987).

Comprehensive experimental and theoretical studies of MTP's have led to a good understanding of their structure and properties. A case treated in detail is that of the pentagonally-twinned decahedral particle. Its formation can be explained by a balance between surface and strain energy. The lowering in total surface energy by exposing ten low-energy {111} faces of the crystal is achieved at the expense of introducing five elastically strained twins within the particle (Ino 1966, Marks 1984). The question of direct relevance to the present work is how the strain associated with the residual 7.35° wedge of material remaining after a five-fold twinning operation, is accommodated. For small particle sizes the strain can be distributed amongst the five twins and accommodated elastically. As the size increases several other possibilities exist for the relaxation of the strain by plastic processes some of which have been directly observed by high resolution TEM. One mechanism is by introduction of a low angle tilt boundary into one of the twin segments with the dislocations spaced at intervals of $h = \theta/b$, where b is the Burgers vector and $\theta = 7.35°$. Examples of this type of accommodation have been observed by Iijima (1987) in twinned spheres of silicon crystallized from the molten state.

Another accommodation mode already observed in Ge precipitates in Al (Dahmen and Westmacott 1986a) is by the radial insertion of extra half planes into the structure between twin segments. It is interesting to note that in this case the inserted half planes are symmetrically disposed so as to preserve the overall symmetry of the orientation relationship.

A third method for filling the 7.35° gap would be by a variety of slip or twinning operations on the conjugate systems in one or more of the twin segments. To completely fill the gap by uniform deformation of one segment only would require the formation of a 15 R polytype if the deformation took place by partial dislocations. In practice it is more likely that more than one segment would be deformed and that a combination of microtwins, stacking faults and perfect dislocations would provide the necessary deformation. In addition to conservative plastic processes, non-conservative growth mechanisms will probably also contribute to the total accommodation.

While it is useful to compare the structures of MTP's formed by vapor deposition and solid state precipitation, the presence of a constraining matrix in the latter case will lead to differences in morphology. As pointed out earlier, the needle morphology develops by virtue of the small mismatch (transformation strain) between the $<110>_{Ge}$ and the $<100>_{Al}$ direction. Maintaining these alignments imposes axial symmetry on the precipitate and its substructure. It is interesting to observe how the precipitate or its different twin segments satisfy one of the OR's with the matrix shown in figs. 1, 3 and 4. In the precipitate/matrix interfaces parallel to a needle axis, the Ge frequently exposes {111} faces to the Al matrix. However, it has been shown elsewhere (Dahmen and Westmacott 1986b) that this is only true within the constraints imposed by the symmetry of the orientation relationship.

During an in-situ treatment, precipitates also nucleate on the surface (fig. 6), leading to a depleted layer and precipitate-free zone parallel to the surface. Their contrast indicates that they are always multiply twinned and commonly have a center of five-fold symmetry.

A variety of cross sectional shapes was found for both the $<100>_{Al}$ and $<110>_{Al}$ needles. Interpretation of the different morphologies is based on the hypothesis that the initial nucleus is either singly twinned (Westmacott and Dahmen 1987) or pentagonally twinned (Dahmen and Westmacott 1986a) and that the possible basic OR's are those depicted in figs. 1 and 4.

4.1. *<100> Needles*

Multiply-twinned precipitates (MTP) are the most frequent configuration, and needles containing five twins along a common $<110>_{Ge}$ axis can be observed after both bulk and in-situ heat treatment. Figure 7(a) shows a high resolution micrograph of the cross-section of a MTP found in a bulk-aged sample. The $<110>_{Ge}$ axis of the needle is parallel to a $<100>_{Al}$ direction. As already reported by Westmacott and Dahmen (1987), the faceting of the precipitate occurs mostly on $\{111\}_{Ge}$ planes and usually exhibits contrast consistent with twinning or a change in stacking sequence at the interface between the aluminum and germanium. Five internal twin-related

segments are denoted 1-5. Segments 1 and 5 obey OR 1(c), the most commonly found OR in <100> needles, and make up the largest part of the precipitate. Segment 3 is relatively small, shares a common {001} plane with the Al matrix (OR 1(a)) and is elastically distorted. Segment 4 is very small and strongly distorted. Since the five twins converge exactly at a point, the intersection area has a special crystallography. Figure 7(b) is an enlargement of this area : the twins meet in a common center imaged as a five-member ring of (black) Ge atom pairs. A model of this configuration is shown in fig. 7(c) and for comparison with the experimental image the corresponding image simulation in fig. 7(d). This kind of ring has already been identified as the origin of the five-fold symmetry of vapor-deposited diamond particles (Matsumoto and Matsui 1983, Angus and Hayman 1988) or silicon particles (Iijima 1987) and germanium precipitates (Dahmen and Westmacott 1986a). They also have been directly observed in materials with diamond or face centered cubic structure, for example during the crystallization process of amorphous silicon (Li and Guo 1985) and as part of higher order twins (e.g. $\Sigma = 9$) in germanium (d'Anterroches and Bourret 1984, Skrotzki, Wendt, Carter and Kohlstedt 1988), as well as in silver (Jefferson and Kirkland 1988).

Another example of a MTP is given in fig. 8. Four different twin-related segments can be observed. The labelling corresponds to the notation used in fig. 7. In this particle, segment 3 which was small in fig. 7, is relatively large and undistorted. Segment 1 is negligibly small and its twin, segment 5 is relatively small as well. None of the segments shows a clear elastic distortion; but notice the alternating 2/3 and 4/5 bands of twins that appear to be correlated across the 3/4 twin boundary.

Two other types of precipitate observed in a <100> zone axis are illustrated in figs. 9 and 10. Unlike the previous examples, these precipitates have a more lath-like character. Only four twin-related segments are observed in fig. 9, and the precipitate in fig. 10 is altogether untwinned. In fig. 9 segment 3 occupies the bulk of the particle. By its shape and OR the central triangular section (segment 3) at the top of this particle is easily identified with its counterparts in figs. 7 and 8. As

in the previous particles this segment is flanked by its twins 2 and 4. However, instead of following these twins with segments 1 and 5 this particle reverts to twin 3. The resulting morphology is distinctly different from the preceding ones.

A small piece of segment 1 is visible near the highly distorted center of the particle and in the enlarged view shown in fig. 9 (b) this shows the familiar fivefold geometry (arrowed). However, this segment does not make a significant contribution to the overall particle morphology.

Fig. 10 consists entirely of segment 3 and contains no twins at all. This is a relatively rare occurrence and from micrographs such as this it could not be determined whether the true shape of the particle is that of a lath or a plate. The faceting is now quite pronounced and it is interesting to note that the major facets are not of the $\{111\}_{Ge}$ type, as in vapor deposited particles, but of the $\{100\}_{Ge}$ type with only minor $\{111\}_{Ge}$ facets at the edge of the particle.

From the examples shown in the preceding micrographs it is clear that there is a correlation between the twin substructure of a particle and its morphology. The majority of the precipitates are similar to that in fig. 7 which is dominated by the OR 1(c). These usually exhibit pronounced facets on $\{111\}_{Ge}$ faces that lie opposite either $\{100\}_{Al}$ or $\{310\}_{Al}$ planes. From this frequent observation it would be tempting to conclude that the morphology is determined by the same surface energy principles as that of vapor-deposited particles. However, note that segment 3 which has the OR 1(a), always tends to facet on the $\{100\}_{Ge}$ face it has in common with the Al matrix, even when it is small. In contrast, segments with an OR of lower symmetry often grow to such shapes as to expose $\{111\}_{Ge}$ faces, see for example segment 4 in figs 8 and 9. This faceting is usually not carried to the extreme of sharp corners. In fact, in all particles examined the junction of $\{111\}_{Ge}$ facets was found to be rounded off. When a segment is small such as twin 5 in fig. 8 this can result in a nearly half-circular shape.

A feature common to all $<100>_{Al}$ precipitates examined is the fact that all can be described as a grouping of the same five twin-related segments with different segments grown to different proportions.

Segment 3 has an outstanding role as the twin with the OR of the highest symmetry, i.e. the Bain relationship, OR 1(a). Segments 1 and 5 obey OR 1(c) which has been shown to be related (to within 3.67°) to segment 3 by secondary twinning. This small misorientation is half the angle of the missing 7.5° wedge that results when five twin segments are joined at a common apex. When several twin segments are present the closure of this wedge angle appears to pose a problem. The parallel twin lamellae seen in fig. 9 and the distortion of the smallest segments, seen in fig. 7 are related to this wedge angle.

The most perfect example of a pentagonally-twinned particle was shown elsewhere (Dahmen and Westmacott 1986a). In this precipitate the 7.5° wedge angle was filled by symmetrical radial insertion of extra half planes on the boundaries between segments 1/2 and 4/5.

4.2. *<110> Needles*

In an analogous manner to $<100>_{Al}$ needles, $<110>_{Al}$ needles also display several different morphologies. Because in both cases the needle axis lies along a $<110>_{Ge}$ direction it is again possible to resolve the substructure, morphology and orientation relationship in high resolution micrographs that show the needle structure in cross section. Several representative particles are described in this section. All observed OR's can be rationalized, and the different twin segments are labelled, with reference to fig. 4.

It is evident from an examination of the low magnification micrograph in fig.5(c) that $<110>_{Al}$ needles frequently exhibit pentagonal twinning. Such precipitates have a characteristic "dog-bone" shape as illustrated in figs. 11 and 12. Segment 3 in figs. 11 and 12 exhibits the cube-cube relationship OR 4(a) while segment 2 follows the cube-twin OR. The main difference between the two particles in figs 11 and 12 lies in the degree of development of segments 4 and 5 and the substructure of parallel twin bands. Segments 4 and 5 are well-developed in fig. 11 and the parallel twin bands are of the type 4/3 and 1/5. In Fig 12 segments 4 and 5 are both equally undeveloped and thin parallel twin bands are of the type 1/2 and 3/4. Figure 12(b) is an enlargement of the

region in which the five twins intersect. The convergence of the five twin segments in a common center is clearly visible. The twin boundaries are marked with arrows and because in this region all twins meet coherently on $\{111\}_{Ge}$ planes they must be elastically distorted to close the 7.5° wedge angle.

Figures 13a and b are two examples of needles that at first sight appear to display no rational OR with the matrix. However, closer inspection shows that segment 4 of fig. 13a is related to the OR depicted in fig. 4(d) by tertiary twinning and segment 5 by quaternary twinning (see fig. 13(c)). In fig. 13b, segments 2 and 3 are related to OR 4(b) by primary and secondary twinning respectively, as shown in fig. 13(d). Thus, each case is related to a primary OR by a sequence of twinning operations.

The morphology of the $<110>_{Al}$ needles is quite similar to that of $<100>_{Al}$ needles: the external shape is related to the internal defect substructure by a tendency for faceting on $\{111\}_{Ge}$ planes. This leads to V-shaped notch on the thin end of the "dog-bone" morphology. The tendency towards $\{111\}_{Ge}$ facets is clearly most pronounced for segments 2 and 3 which have OR with high symmetry. Most other segments are rounded, possibly due to their smaller size.

§ 5. DISCUSSION

5.1. *Importance of Twinning*

The results shown in the preceding sections illustrate the great variety of orientation relationships and morphologies that are observed in quench-aged Al-Ge alloys. Throughout the presentation of the experimental results the relationship between the twin substructure of a precipitate and its morphology has been emphasized. Twinning appears to be present at least once in almost every precipitate and it is clear that twinning is intimately related to nucleation and growth. This is true for the observations on needle-shaped precipitates presented here as well as

for plate-shaped precipitates examined previously. Very similar results are found for Al-Si alloys which exhibit the same spectrum of morphologies and the same ubiquitous twinning. Furthermore, a comparison between the substructures of $<100>_{Al}$ and $<110>_{Al}$ needles shows that fivefold twinning appears to play a special role. It is interesting to see that the bewildering variety of OR's can be related to just three basic relationships through multiple twinning operations.

The Ge frequently exposes {111} faces to the Al matrix, as is found in vapor deposited particles. However, due to the orientation relationship with the surrounding matrix, equivalent {111} faces of the Ge will often see nonequivalent faces in the Al. In well-developed particles with equilibrium shapes, {111} faceting is therefore found only within the constraints imposed by the composite symmetry of the orientation relationship (Cahn, Kalonji 1981), and precipitates with high-symmetry orientation relationships often display large {100} or {110} facets. Furthermore the observed precipitates do not approximate spheres, as in vapor deposited decahedral or icosahedral particles, but needles or laths. Where they are bounded by {111} faces these are parallel to the needle axis rather than inclined as in a decahedron.

5.2. *Lattice Correspondence*

The fact that orientation relationships are observed at all implies some interaction between the Al matrix and the Ge precipitates that makes crystal alignments preferable to random orientation. However, it is difficult to find a reasonable lattice correspondence between the face centered cubic (fcc) Al and the diamond cubic (dc) Ge lattice. Because the motif of the dc lattice has twice the number of atoms of the fcc lattice, two unit cells of the Al lattice must correspond to one cell in the Ge lattice for a conservative lattice correspondence (conserving the number of lattice sites). The simplest way of accomplishing this is the correspondence shown in Figure 14(a), which is similar to the Bain correspondence in the fcc/bcc case: the lattices are aligned along a common cube axis and rotated by 45° relative to each other about that axis. The transformation strain is relatively small and uniform in the common cube face: $\frac{a_{Ge}}{\sqrt{2}a_{Al}} = 0.989$. On the other hand, along the

common cube direction, the strain is large: $\frac{a_{Ge}}{a_{Al}} = 1.399$. The principal distortions of the transformation strain matrix are thus (0.989, 0.989, 1.399) when referred to the cube axes of the Al matrix. However, due to the large 36% volume increase, precipitation without vacancies is not possible. This has been found repeatedly and reproducibly in precipitate-free-zones near grain boundaries and other vacancy sinks. Vacancies may thus be thought of as integral part of any operating lattice correspondence. One suggestion has been the incorporation of as many as 50% vacancies in a lattice correspondence with the same relative lattice orientation as the one described above (Khachaturyan, 1986). If one half of the atoms in each {001} layer are replaced by vacancies, two Al unit cells will collapse to one dc unit cell, see fig 14(b). The transformation strains would then be (0.989, 0.989, 0.699).

These two are extreme cases since one lattice correspondence incorporates substantially more vacancies (50%) than required for complete volume accommodation (36%), and the other one none at all (conservative). In either case appreciable strain will have to be accommodated by lattice deformation, an expansion for the conservative case and a contraction for the non-conservative case with 50% vacancies.

Other lattice correspondences can be searched out with the aim of incorporating close to the required number of vacancies and thus minimizing the accommodation strain. This is the procedure followed in the near coincidence-site lattice approach, usually applied to two-dimensional interfaces, (Zur and McGill, 1983, Gao, Shewmon and Dregia, 1988) but easily extended to three dimensions. The aim here is to find a near-CSL cell that is small enough to have physical significance and incorporates nearly the required number of vacancies thus needing only small transformation strains. For Al-Ge, one such correspondence is that shown in Figure 15. If the two lattices are in parallel (cube-cube), OR, then a near coincidence is established every 7 spacings (5 Ge spacings). In two dimensions (planar coincidence site lattice) this is commonly denoted as $\Sigma 5/7$, and in 3 dimensions this becomes $\Sigma 125/343$. The residual strain is minimal (0.1%), compared to the largest strain of the conservative correspondence (39.9%). However, the

number of atoms in such a coincidence cell is large, i.e. only 1 in every 343 Al atoms (250 Ge atoms) is related in this way (as opposed to 1 in 2 atoms for the case of the conservative correspondence).

In actual precipitate growth an interesting variation on this principle is found: Si plates that form in cube-cube OR on {111} planes of the Al matrix assume the planar near-CSL lattice correspondence in the habit plane but maintain a 1:1 correspondence normal to the habit plane. This is evident from the strain contrast that develops as the plates thicken. A <110> interstitial strain field similar to that of a prismatic dislocation loop builds up until it is relieved by the precipitation of a layer of vacancies (Westmacott and Dahmen, 1987). A point of interest about this observation is that the developing strain field has a shear component parallel to the habit plane, therefore it could exert a bias on subsequent twin formation. The implications of this will be discussed in section 5.3

Another possible lattice correspondence is shown in Figure 16. This is designated as the inverse Bain correspondence. Here, the mismatch along the common <110> direction is large and that in the common {110} plane is small.

Many other possible near-CSL orientations and lattice correspondences could be found by using a computer algorithm (Zur, McGill, 1983, Chen, 1988) However, since no criteria for optimization have been established, the usefulness of such an exercise is doubtful without further reference to experimental observation.

A common factor in all needle and lath morphologies is the perfect lattice alignment along the needle axis as opposed to the many different orientations about this common zone. Close inspection of the contrast behavior of the precipitates confirms this difference: along the needle axis there is evidence of dislocations and localized strains whereas no dislocations could ever be identified in any of the high-resolution images of cross sections viewed along the needle axis. The absence of dislocations in the cross-sectional images is in contrast to the structures found for many oxide precipitates in a metal matrix (Mader, 1989; Kubawara, Spence, Rühle, 1989), although in

some metal/oxide systems similar "incoherent" interfaces are observed (Mader, 1989, Muschik, 1989). It appears that for $<100>_{Al}$ needles the correspondence cell is a hybrid of a conservative atom-by-atom correspondence along the needle axis $<100>_{Al} \parallel <110>_{Ge}$ with a near-CSL correspondence normal to the needle axis. {111} plate precipitates observe a similar hybrid correspondence with a near-CSL lattice in the habit plane and a 1:1 atomic correspondence normal to the habit (Westmacott and Dahmen, 1987).

5.3. *Vacancies and Twinning in the Morphological Development*

The relationships between different OR's, twinning and morphologies developed above can be used to paint a coherent picture of the growth of precipitates that unifies all the diverse observations made on this alloy system. The simplest OR is the cube-cube relationship illustrated in fig. 15. In Al-Si alloys it has been observed that with this OR precipitates form mainly plates on common {111} planes. This observation may be described by a vacancy/Ge atom coprecipitation mechanism advanced earlier. For plates to nucleate it is assumed that a high local vacancy concentration is necessary. This is because the plate must exceed a critical size before the associated Ge atoms can pucker into the DC structure. However, precipitate growth normal to this plane is difficult because the interstitial strain that builds up with every Ge layer is large and must be relieved periodically by the incorporation of vacancies. A similar mechanism can be postulated for {100} plates with the Bain correspondence. In the common {100} plane a 1:1 atomic correspondence with a small transformation strain allows for a good match. Furthermore, the OR of fig. 1(c) 100 Al ∥ 111 Ge, might also nucleate by coprecipitation on {100} Al. In each case further precipitate growth occurs by a ledge mechanism, and the rate of growth will depend on the vacancy diffusion coefficient.

Plate growth for the cube-cube and the Bain correspondence is shown schematically in figs. 17 and 18 (a). The morphology on a {111} plane would be that of a hexagonal or triangular plate

whereas that on a {100} plane would be square or rectangular plate. An untwinned {100} plate in cross section would look like the particle in fig.10. Twinning parallel to the habit plane without effect on the plate morphology is possible and has been seen only for {111} plates (Dahmen, Douin, Hetherington and Westmacott, 1989). Such a twin parallel to the {111} habit plane is illustrated schematically in fig. 17 (a). For {111} plates this particular twin orientation is also favored by the bias due to the shear component of the transformation strain.

If accidental twinning occurs on one of the other twin systems of the {111} plates, or on any twin system of the {100} plates, the lattice correspondence that is responsible for the plate shape will not be maintained. The plate morphology will be locally disturbed as shown in figs. 17 and 18 (b). Further growth of the twinned segment will be difficult, and it is likely that the next developing twin is one that reverts to the original orientation. This would lead to plates or laths such as that shown in fig. 9.

If the local vacancy concentration is low or if twinning occurs early in the growth of a precipitate it is possible that other morphologies develop. This is illustrated schematically in figs. 17 and 18 (c). Once the first twin that destroys the high-symmetry OR necessary for plate growth has been formed the only easy growth direction that remains from the original habit plane is the common <110> direction in fig. 18 and the $<110>_{Ge}/<100>_{Al}$ direction in fig. 17. Further twinning is now possible within the same $<110>_{Ge}$ zone without destroying the lattice match along the common growth direction. It is easy to see how only five distinct twin segments can be formed from each high-symmetry lattice correspondence and how their relative development depends on the sequence of twinning. During radial growth of these needles or laths vacancies can be added slowly as needed. The morphologies seen in figs. 7, 8, 9, 11 and 12 can be rationalized in terms of such a sequence of events.

Finally, it is possible that during the lengthening of a needle or lath one or more of the original twin segments is discontinued, as shown schematically in fig. 18 (d). When such a needle is seen in cross section it will often show an irregular morphology and an irrational OR of the twin-related

segments with the matrix. Such needles are seen in figs. 13a and b. The primary OR to which they are related by multiple twinning (Inverse Bain) was found very infrequently and the possibility of plate growth on common {110} planes under conditions of high vacancy concentration, analogous to {111} and {100} plates for the cube-cube and Bain correspondences, has not be examined experimentally. However, it is likely that a similar transition from plates to laths or needles occurs for this case as well when the local vacancy concentration changes.

5.4. *Vacancies and Twinning in Nucleation*

In the preceding discussion attention has been focused on understanding the morphologies that develop during precipitate growth in terms of accidental multiple twinning. A simple relationship between the precipitate type and the local vacancy concentration was hypothesized. The great variability of shapes and OR's were simply determined by different twinning sequences during growth. However, the role of twinning in the nucleation stage has not been addressed explicitly so far. Although in previous work (Westmacott and Dahmen, 1987) a twinned nucleus for the case of $<100>_{Al}$ needles was proposed, the possible function of twinning in the nucleation stage remains to be evaluated systematically.

In order to accommodate the large disparity in the atomic volumes of aluminum and germanium (16.6 $Å^3$ vs. 22.6 $Å^3$), precipitation and growth need an excess of vacancies, usually introduced by quenching (Russell 1969, Dahmen and Westmacott 1986b, Beller 1972). The ease of nucleation will be proportional to the concentration of vacancies. The lower the need a particular configuration has for vacancies, the more favored the precipitation will be. Thus it is postulated that nucleation occurs by a process which tends to reduce the number of vacancies used by increasing the number of Ge-Ge bonds per atom for a given number of atoms per nucleus. The possible configurations that satisfy this condition in the diamond-cubic structure can be constructed systematically . As shown in fig. 19, when the number of atoms involved is 8, 10 or

12, special closed configurations, or cages, appear (fig.20) which have a higher density of the precipitate nucleus.

The first complete nucleus with maximum density is the eight-atom cage drawn in fig. 20(a). As described by Angus and Hayman (1988) for the diamond structure, this nucleus consists mainly of six-membered rings with the so-called boat configuration and its extension will lead to a twinned crystal. This is not the case for the second cage in which ten atoms forming six-membered rings constitute the chair configuration known to give rise to an untwinnned crystal (fig. 20(b)). The third configuration with twelve atoms (fig. 20(c)) is in fact the continuation of the first configuration with eight atoms, as the fourth is the next step after the ten-atom cage, and so on.

Since the precipitation occurs in the aluminum matrix a nucleus is constrained by the condition of good match with the matrix. This match is illustrated for each nucleus configuration in fig.21. Again, the twinned configuration appears more favorable since for a greater number of germanium atoms (14 against 12) in the same volume it needs one less vacancy.

It is clear from this discussion that twinning has a dual role in the formation of Ge precipitates in Al: during nucleation it serves to maximize the number of Ge-Ge bonds and thus reduce the initial need for vacancies, whereas during growth accidental twinning strongly influences the developing morphology.

§ 6. CONCLUSIONS

The major result of the present study can be summarized as follows:

(1) only few different orientation relationships and their twin-derivatives are experimentally observed.

(2) both $<100>_{Al}$ and $<110>_{Al}$ needle precipitates are usually twinned and the many different observed cross-section morphologies can be explained by the development of five cozonal twins in different proportions.

(3) all observed morphologies can be rationalized by different local vacancy concentrations and different sequences of multiple twinning.

(4) the predominant factors for the formation of the nucleus are the demand for vacancies and the minimization of the strain energy. The configuration which appears to follow these criteria best consists of only eight atoms and invariably leads to the formation of a twinned crystal.

ACKNOWLEDGEMENT

We would like to thank C. Nelson for his assistance with the Atomic Resolution Microscope and C.J.D. Hetherington for helpful comments on the manuscript.

This work is supported by the Director, Office of Energy Research, Office of Basic Energy Sciences, Materials Sciences Division of the U.S. Department of Energy under contract No.DE-AC03-76SF00098.

REFERENCES

Angus, J.C., and Hayman, C.C., 1988, *Science*, 241, 913.

d'Anterroches, C., and Bourret, A., 1984, *Phil. Mag. A*, 49, 783.

Beller, M., 1972, *Z. Metallk.*, 63, 663.

Cahn, J.W., and Kalonji, G., 1981, Proc. Int. Conf. Solid State Phase Transf. (Pittsburgh, PA), p.3.

F.-R. Chen, 1988, private communication

Dahmen, U., Douin, J., Hetherington, C.J.D. and Westmacott, K.H., 1989, *Proc. MRS Symp.*, 139, 87 (eds. W. Krakow, F.A Ponce and D.J. Smith)

Dahmen, U., Nelson, C., and Westmacott, K.H., 1986, *Proc. 44th EMSA*, 538 (ed. G.W. Bailey).

Dahmen, U., Pelton, A.R., Witcomb, M.J., and Westmacott, K.H., 1981, *Proc. Conf. Solid-Solid Phase Transf.*, Pittsburgh, PA, p.637, (eds. H.I. Aaronson, D.E. Laughlin, R.F. Sekerka and C.M. Wayman).

Dahmen, U., and Westmacott. K.H., 1986a, *Science*, 233, 875 ; 1986b, *Proc. MRS Symp.*, 62, 217 (eds. L.W. Hobbs, K.H. Westmacott and D.B. Williams); 1989, *J. Electron Micr. Techn., submitted*

Y. Gao, P. Shewmon and S.A. Dregia, 1988, *Scr. Met.*, 22, 1521

Gouthama, G.N., Subbana, and Kishore, 1985, *Mat. Sci. Forum*, 3, 261.

Gouthama, G.N., and Kishore, 1987, *Proc. Phase Transf. Conf*, Cambridge, England (in press).

Gouthama, G.N., 1989, private communication

Hugo, G.R., and Muddle, B.C., 1986, Research Report, Monash University.

Hugo, G.R., and Muddle, B.C., 1989, submitted for publication (private communication).

Iijima, S., 1987, *Japan. J. Appl. Phys.*, 26, 357, and *ibid.*, 365.

Ino, S., 1966, *J. Phys. Soc. Jap*an, 21, 346.

Ino, S., 1969, *J. Phys. Soc. Japan*, 27, 941.

Jefferson, D.A., and Kirkland, A.I., 1988, *Proc. IOP short meet.*, "Electron Beam Imaging of Non-Crystalline Materials" (ed. K. Knowles, London), p.71.

Khachaturyan, A.G., 1986, private communication

Kobayashi, K., Shingu, P.H., and Ozaki, R., 1976, *J. Mater. Sci.*, 11, 399.

Köster, U., 1969, *Mat. Sci. Eng.*, 5, 174 ; 1971, Ph.D Thesis, Göttingen.

Kuwabara, M., Spence, J.C.H.and Rühle, M., 1989, *J. Mat. Res.*, 4, 972

Li, Y., and Guo, K., 1985, *Proc. 3th Chinese-Japanese Elec. Mic. Seminar*, Hanzhou (China) (eds. H. Hashimoto, K.H. Kuo, L. Lee and K. Ogawa), p.71.

Lorimer, G.W., and Nicholson, R.B., 1969, *Inst. Metals Monograph*, 33, 36.

Lu, S.Z., and Hellawell, A., 1987, *Metall. Trans. A*, 18A, 1721.

Mader, W., 1989, *Z. Metallk.*, submitted

Marks, L.D., 1984, *Phil. Mag. A.*, 49, 81.

Matsumoto, S., and Matsui, Y., 1983, *Journal of Mat. Sci.*, 18, 1785.

Mushik, A., 1989, private communication

Heinemann, K., Yacamán, M.J., Yang, C.Y., and Poppa, M., 1979, *J. Cryst. Growth*, 47, p.177.

Ozawa, E., and Kimura, H., 1970, *Acta Met.*, 18, 995.

Rosenbaum, H.S., and Turnbull, D., 1958, *Acta Met.*, 6, 653.

Russell, K.C., 1969, *Scripta Metal..*, 3, 313.

Saulnier, A., 1961, *Mem. Sci. Rev. Metallurg.*, 58, 615.

Skrotzki, W., Wendt, H., Carter, C.B., and Kohlstedt, D.L., 1988, *Phil. Mag. A*, 57, 383.

Westmacott. K.H., and Dahmen, U., 1982, 40th Am. Proc. EMSA (Washington, D.C.), (ed. G.W. Bailey), p.62a; 1985, Mat. Sci. Forum, 3, 325 ; 1986, *Rev. de Physique Appl.*, 21, 757 ; 1987, *Proc. Phase Transf. Conf*, Cambridge, England, 357.

A. Zur and T.C. McGill, 1983, *J. Appl. Phys.* 55, 378

Table 1

Morphology	OR		Ref.	Fig.
Plate on $\{111\}_{Al}$	$\bar{1}11 // \bar{1}11_{Al}$ $110 // 110_{Al}$ $1\bar{1}2 // 1\bar{1}2_{Al}$	Ge, Si	S, K, WD, GK	4a
Hexagonal plate on $\{111\}_{Al}$	$\bar{1}11 // \bar{1}11_{Al}$ $211 // 110_{Al}$ $01\bar{1} // 1\bar{1}2_{Al}$	Ge	H, G	
Plate on $\{001\}_{Al}$	$\bar{1}11 // 001_{Al}$ $110 // 110_{Al}$ $1\bar{1}2 // 1\bar{1}0_{Al}$	Ge	K, GK	4c
Plate on $\{001\}_{Al}$	$111 // 100_{Al}$ $01\bar{1} // 010_{Al}$ $\bar{2}11 // 001_{Al}$	Ge	K,G	1c
Plate on $\{001\}_{Al}$	$110 // 100_{Al}$ $001 // 001_{Al}$ $1\bar{1}0 // 100_{Al}$	Ge	GK	1a
Needle along $[100]_{Al}$	$110 // 100_{Al}$ $1\bar{1}1 // 001_{Al}$ $\bar{1}12 // 010_{Al}$	Ge, Si	K, DNW, GK	1c
Needle along $[100]_{Al}$	$110 // 100_{Al}$ $1\bar{1}0 // 011_{Al}$ $001 // 01\bar{1}_{Al}$	Ge	H, DW(b)	1b
Needle along $[100]_{Al}$	$110 // 100_{Al}$ $001 // 001_{Al}$ $1\bar{1}0 // 100_{Al}$	Ge	DW(b),DDW,K	1a
Needle along $[100]_{Al}$	$110 // 100_{Al}$ $1\bar{1}1 // 01\bar{1}_{Al}$ $\bar{1}12 // 011_{Al}$	Ge	DW(a)	1d
Lath along $[100]_{Al}$	$\bar{1}11 // 001_{Al}$ $110 // 100_{Al}$ $1\bar{1}2 // 010_{Al}$	Ge	H	1c
Needle along $[110]_{Al}$	$110 // 110_{Al}$ $\bar{1}11 // 1\bar{1}1_{Al}$ $1\bar{1}2 // \bar{1}12_{Al}$	Ge	DDW	4a
Needle along $[110]_{Al}$	$110 // 110_{Al}$ $1\bar{1}1 // 1\bar{1}2_{Al}$ $\bar{1}12 // \bar{1}11_{Al}$	Ge	H, DDW	1b
Needle along $[110]_{Al}$	$110 // 110_{Al}$ $001 // \bar{1}11_{Al}$ $1\bar{1}0 // 1\bar{1}2_{Al}$	Si	WD	4c
After eutectic solidification	$001 // 1\bar{1}0_{Al}$ $100 // 11\bar{1}_{Al}$ $010 // 112_{Al}$	Si	KSO, LH	1c
After eutectic solidification	$11\bar{1} // 01\bar{1}_{Al}$ $112 // 111_{Al}$ $\bar{1}10 // \bar{2}11_{Al}$	Si	LH	

Table 1 : Summary of the different Orientation Relationships (OR) of Ge or Si precipitates in Al matrix found in the literature. The observed precipitate morphologies are indicated. DDW : present work, DNW : Dahmen, Nelson and Westmacott 1986, DW : Dahmen and Westmacott, 1986(a), 1986(b); G: Gouthama 1989; GK : Gouthama and Kishore 1987; H : Hugo 1986 ; K : Köster 1969 ; KSO : Kobayashi, Shingu and Ozaki 1976 ; LH : Lu and Hellawell 1987; S : Saulnier 1961; WD : Westmacott and Dahmen 1982(a),1987(b).

Figure Captions

Figure 1 : Schematic illustration of four different OR's found in Al-Ge alloys. The truncated square represents the Al matrix in <100> projection while the inscribed truncated rectangle stands for the Ge precipitate in <110> projection.

Figure 2 : Same OR's as in fig.1. The symmetry elements are indicated by conventional symbols.

Figure 3 : Schematic illustration of the OR's that can be obtained from that of fig.1a (labelled 3) by multiple twinning. The OR labelled 1, reached after two successive twinning operations, is within 3.67° of the OR shown in fig.1 c.

Figure 4 : Schematic illustration of four more OR's found in Al-Ge alloys. The truncated rectangle represents the Al matrix in <110> projection while the inscribed truncated rectangle stands for the Ge precipitate in <110> projection.

Figure 5 : Conventional bright field micrographs showing the morphology of Ge precipitates after bulk aging, (a) and (c), and thin-foil aging (b). In a [001] zone axis, (a) and (b), the alignment of the needles along <100> matrix directions is apparent. Characteristic cross-sectional shapes (circled) resulting from multiple twinning of the needles are seen in $<100>_{Al}$ and $<110>_{Al}$, (a) and (c), respectively. The lines with Miller indices indicate crystal directions.

Figure 6 : Bright field micrograph of precipitates nucleated at the surface during in-situ heating showing extensive internal twinning substructure.

Figure 7 : High resolution image of a [100] needle found in a bulk-aged Al-Ge alloy. (a) general view showing the internal structure with five twins; (b) enlargement of multiply-twinned region of (a); (c)-(d) model and image simulation of the five-atom ring at the intersection of the twins (thickness = 50 Å, defocus = - 800 Å).

Figure 8 : High resolution micrograph of a multiply-twinned particle (MTP) with an almost triangular segment 3 and symmetrically disposed twin bands across segments 3 and 4.

Figure 9: Micrograph of a precipitate with a more lath-like shape. The morphology is dominated by segment 3 and perturbed only slightly by the minor segments 1, 2 and 4.

Figure 10: Micrograph illustrating the lath morphology of the sole example of an untwinned precipitate found in the present study.

Figure 11 : High resolution micrograph of a $<110>_{Al}$ needle with the so-called dog-bone configuration. Most of segment 3 has the cube-cube OR of Fig. 4(a). The multiply-twinned end appears to have pseudo-fivefold symmetry.

Figure 12 : High resolution micrograph of another example of a $<110>_{Al}$ dog-bone needle; the enlargement (b) shows clearly that the intersection of five twins, the boundaries of which are marked T, leads to a five-atom ring of Ge.

Figure 13: High resolution micrographs of two other OR's commonly found in $<110>_{Al}$ needles are shown in (a) and (b). The OR's observed are related to those of Figs. 4 (d) and (b) by multiple twinning as illustrated schematically in (c) and (d) for Fig. 13 (a) and (b) respectively.

Figure 14: Diagrams showing a conservative Bain lattice correspondence requiring an expansion of the Al matrix (a), and an alternative non-conservative Bain correspondence requiring the incorporation of 50% vacancies in the lattice (b).

Figure 15: A near-CSL (Σ 125/343) for a cube-cube lattice correspondence reflects the close atomic match indicated for one set of cube planes between 7 Al and 5 Ge spacings.

Figure 16: Diagram illustrating the Inverse Bain lattice correspondence whereby the Al and Ge lattices share a common <110> direction.

Figure 17: A [111] plate morphology is depicted for a triangular twinned precipitate in (a) and a subsequent twinning event that leaves its plate character unchanged in (b). An alternative morphology and further cozonal twinning that will lead to lath growth is sketched in (c).

Figure 18: Schematic diagrams showing the various effects of twinning on a [100] plate morphology. In (b) the plate morphology is preserved, whereas in (c) and (d) needle morphologies are developed consistent with those observed experimentally.

Figure 19 : Plot of the variation in the number of bonds per atom in the diamond-cubic structure as a function of cluster size for twinned and untwinned nuclei.

Figure 20 : The different configurations pointed out by the curve in fig.19. (a), (b) and (c) correspond to the first three cages ; (d) and (e) are respectively the unit cell and the 15-atom cage related to the five-atom ring.

Figure 21 : Complete unit cells corresponding to the two fundamental cages (fig. 20 (a) and (b)) ; the mismatch between Ge precipitate and matrix as well as the number of vacancies required are indicated.

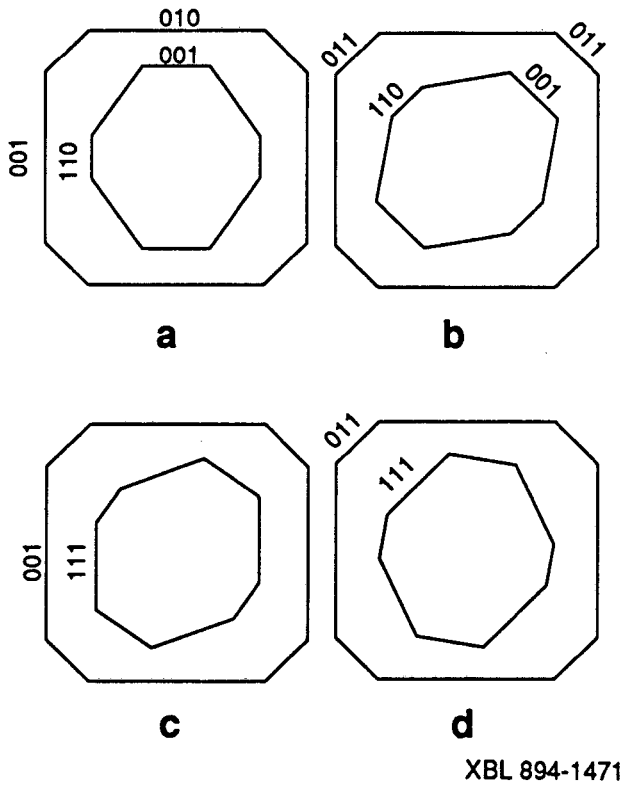
010
001
001
110
a
011
011
001
110
b
001
111
c
011
111
d
XBL 894-1471

Figure 1

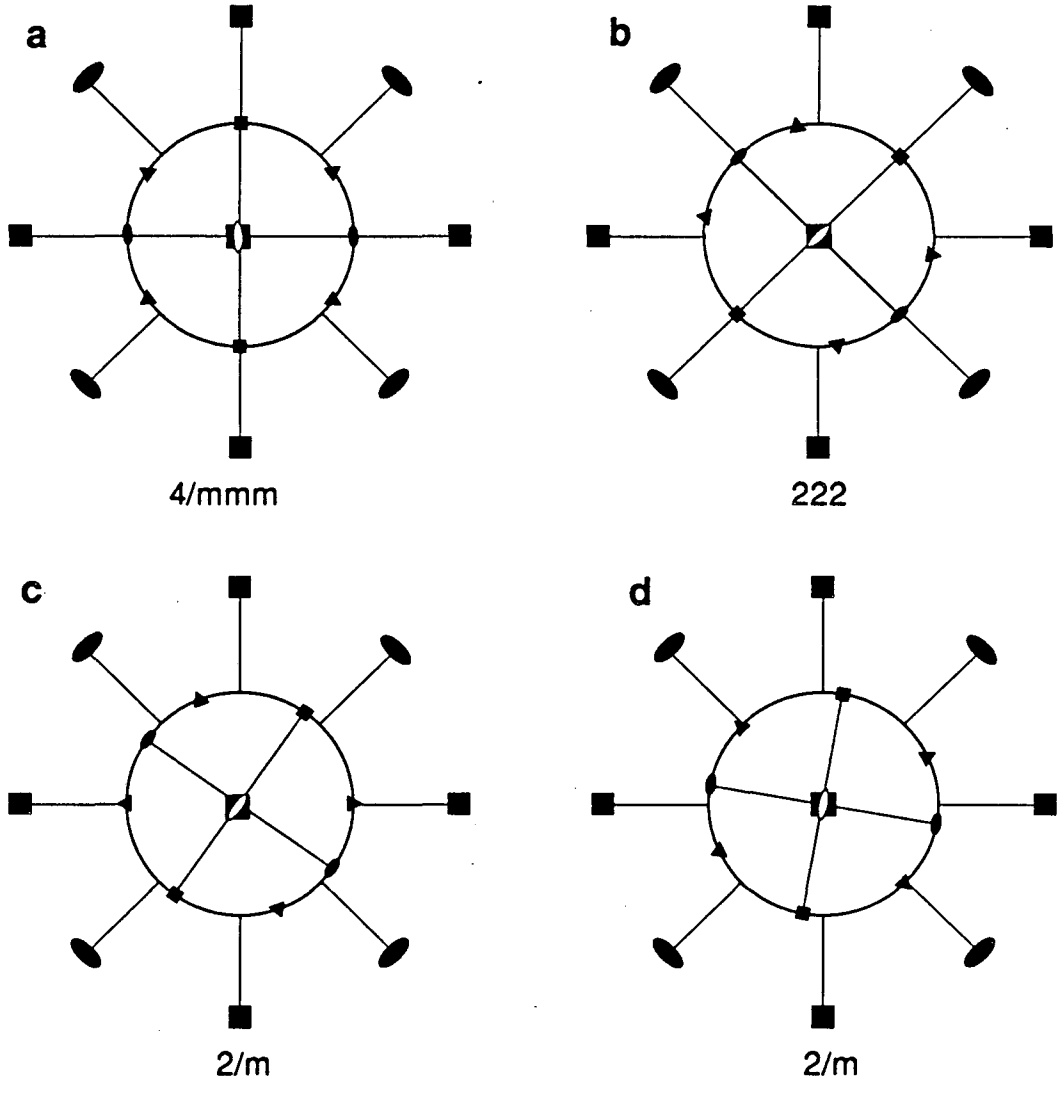

Figure 2

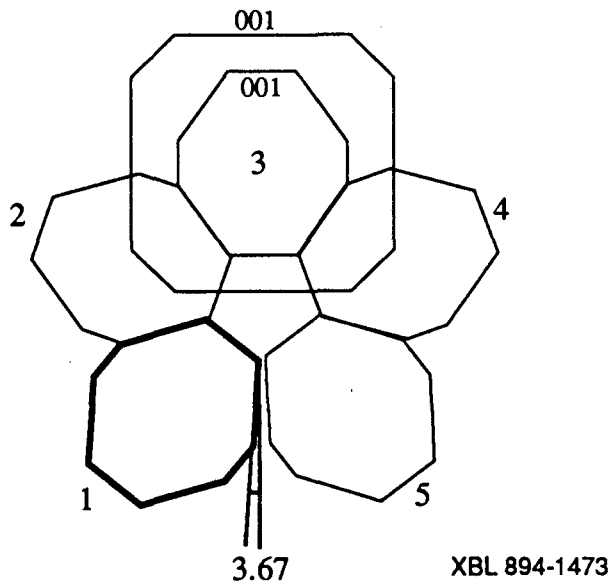

Figure 3

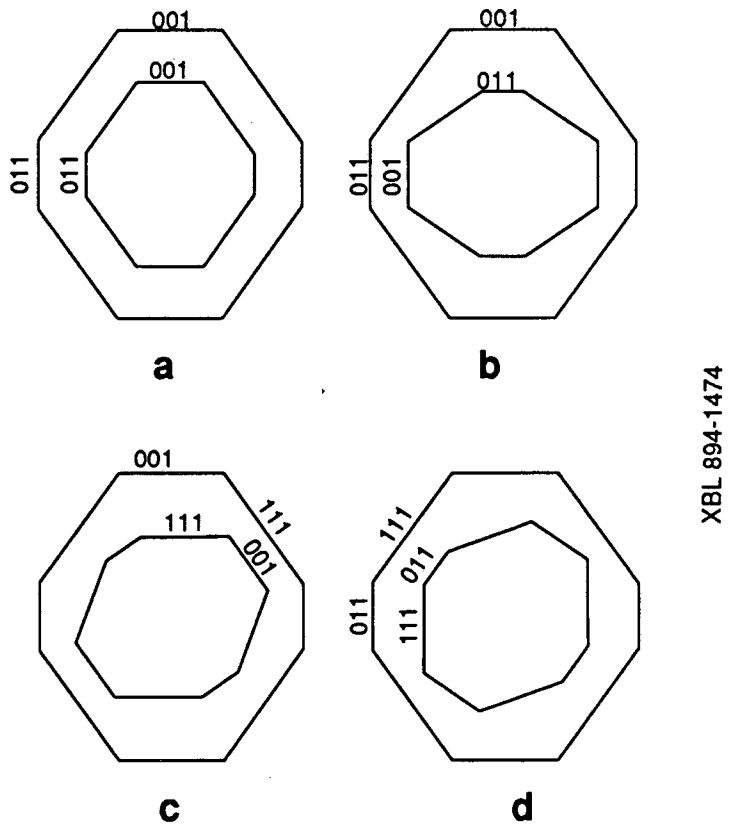
001
001
011
011
a
001
011
011
001
b
001
111
111
001
c
111
011
011
111
d
XBL 894-1474

Figure 4-

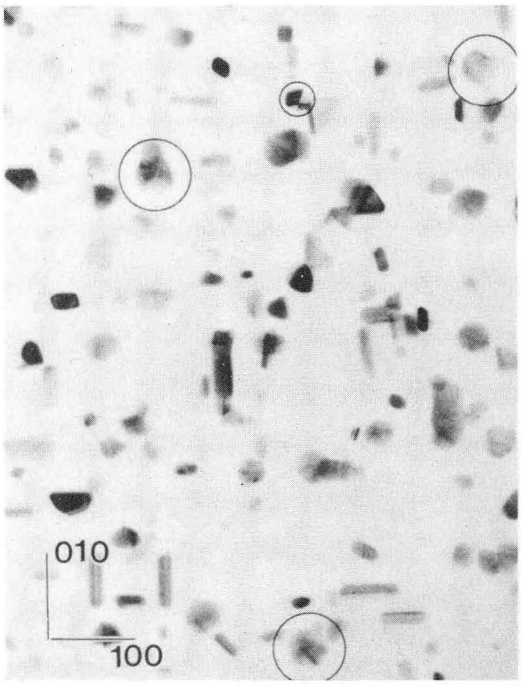

a)

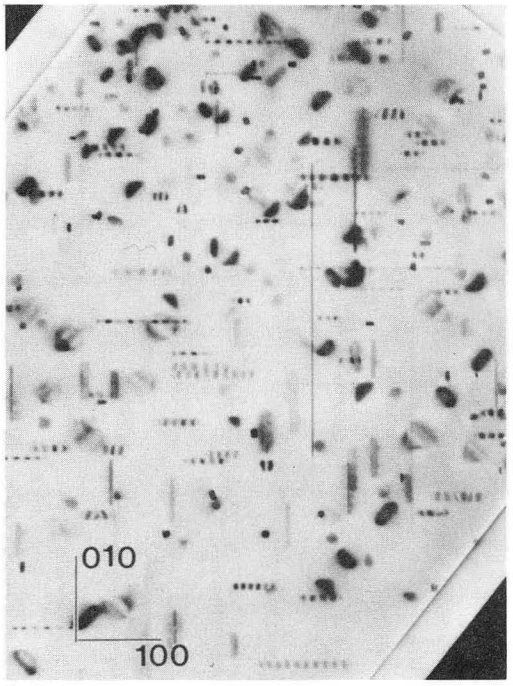

b)

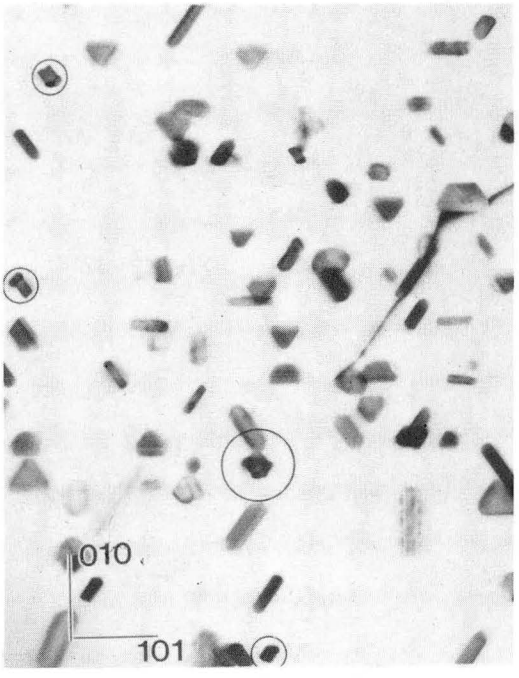

c)

XBB 892-1273

FIGURE 5

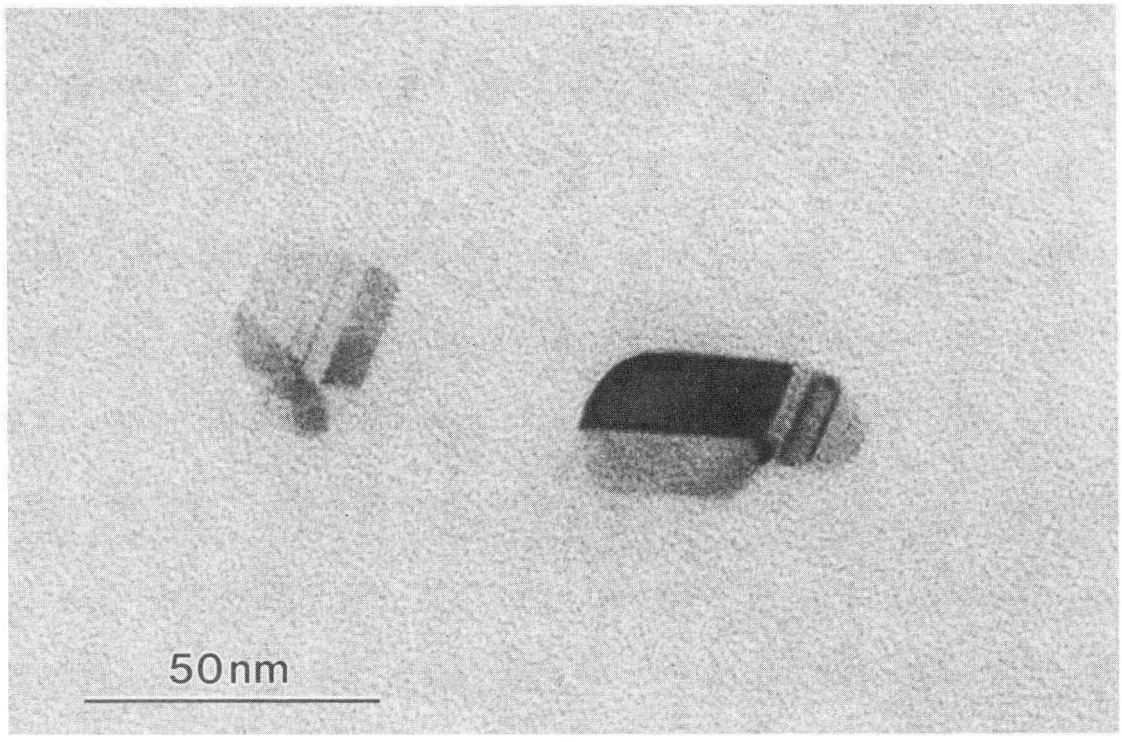

XBB 894-3214

FIGURE 6

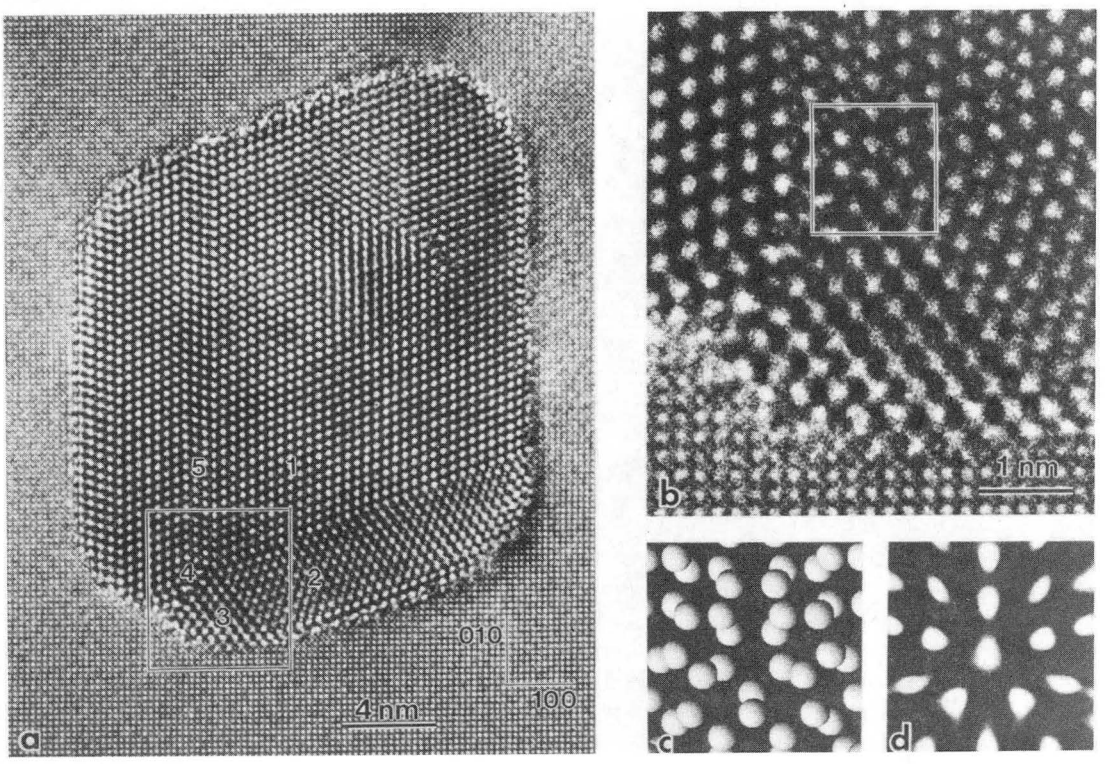

XBB 894-3221

FIGURE 7

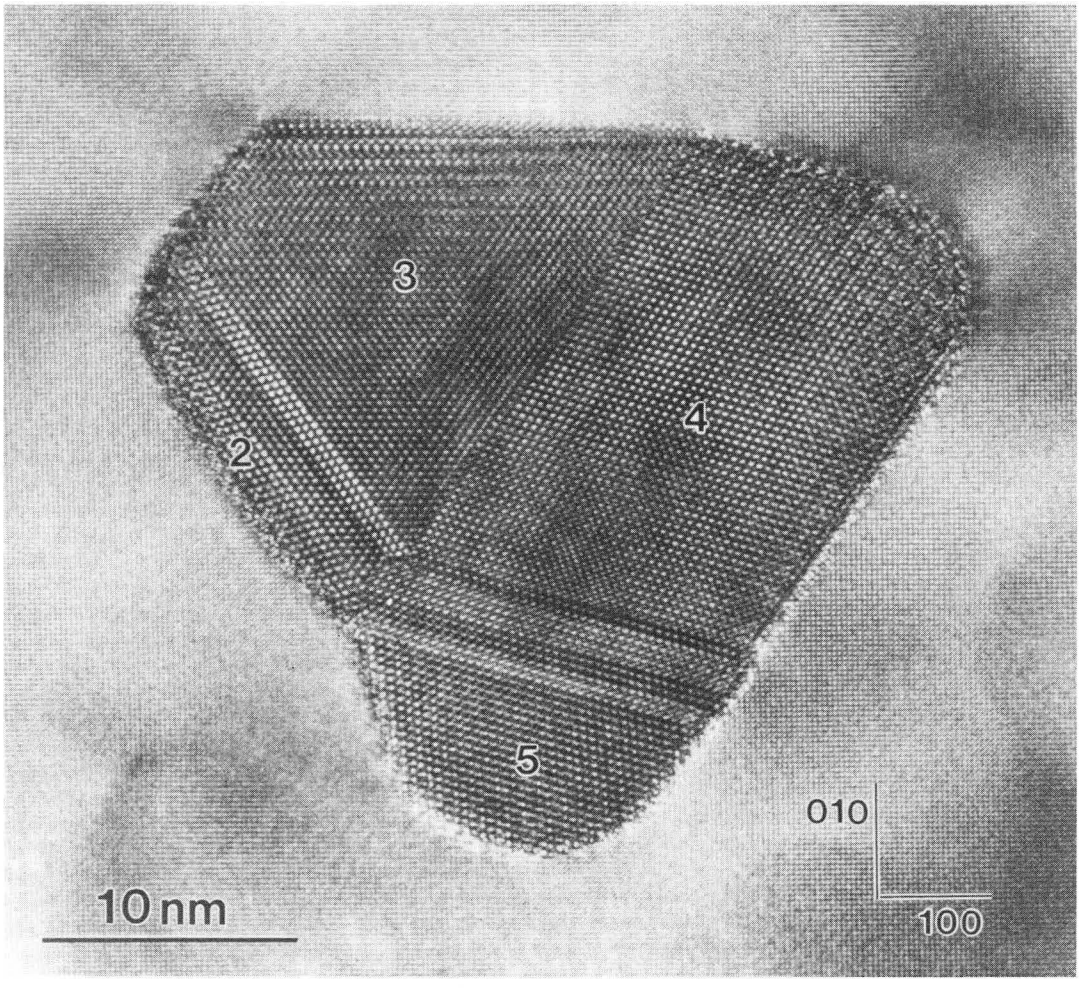

XBB 894-3213

FIGURE 8

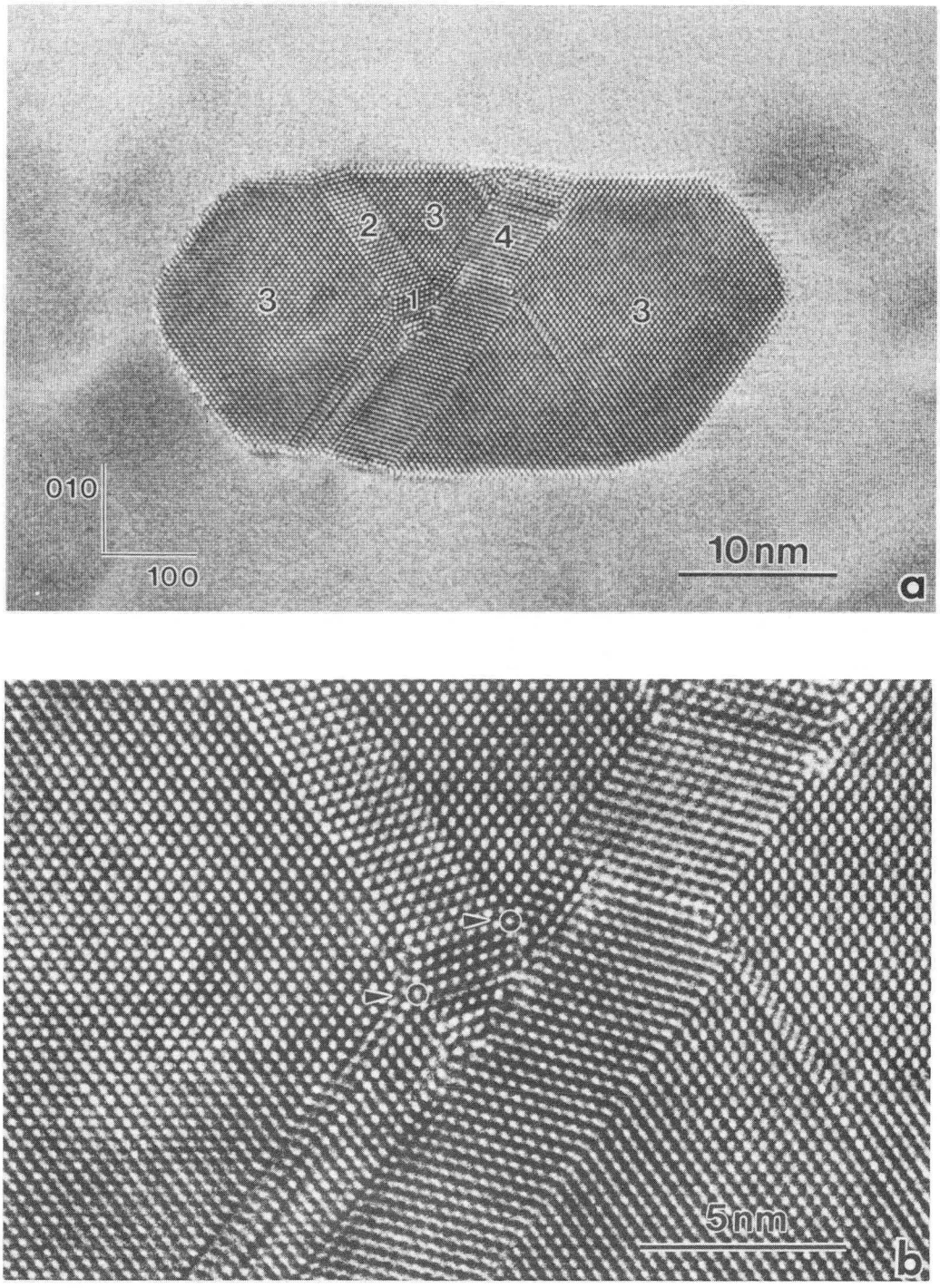

XBB 894-3222

FIGURE 9

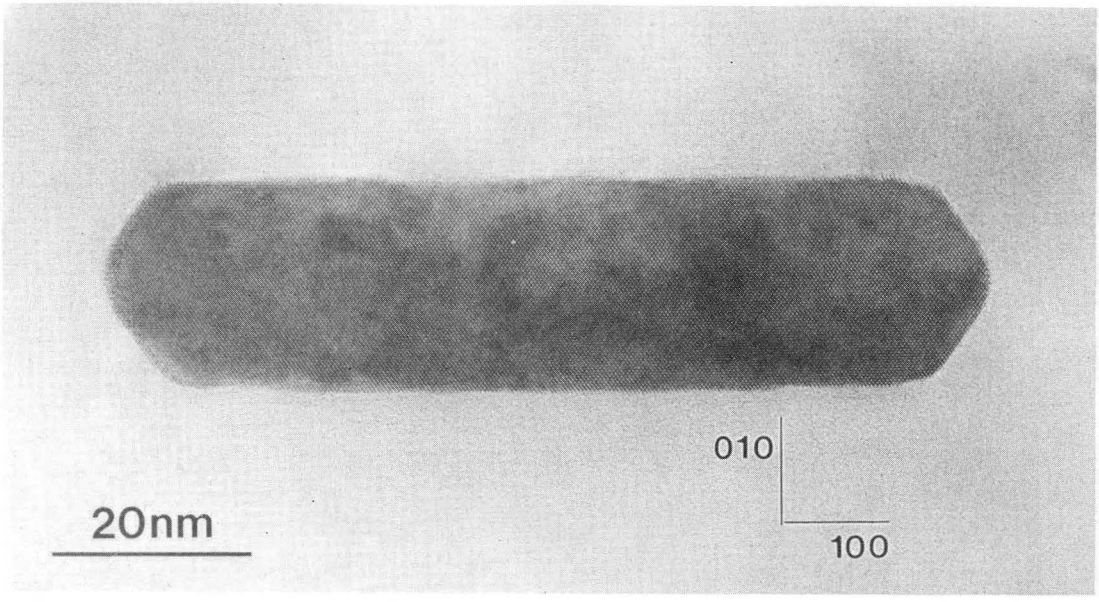

XBB 894-3215

FIGURE 10

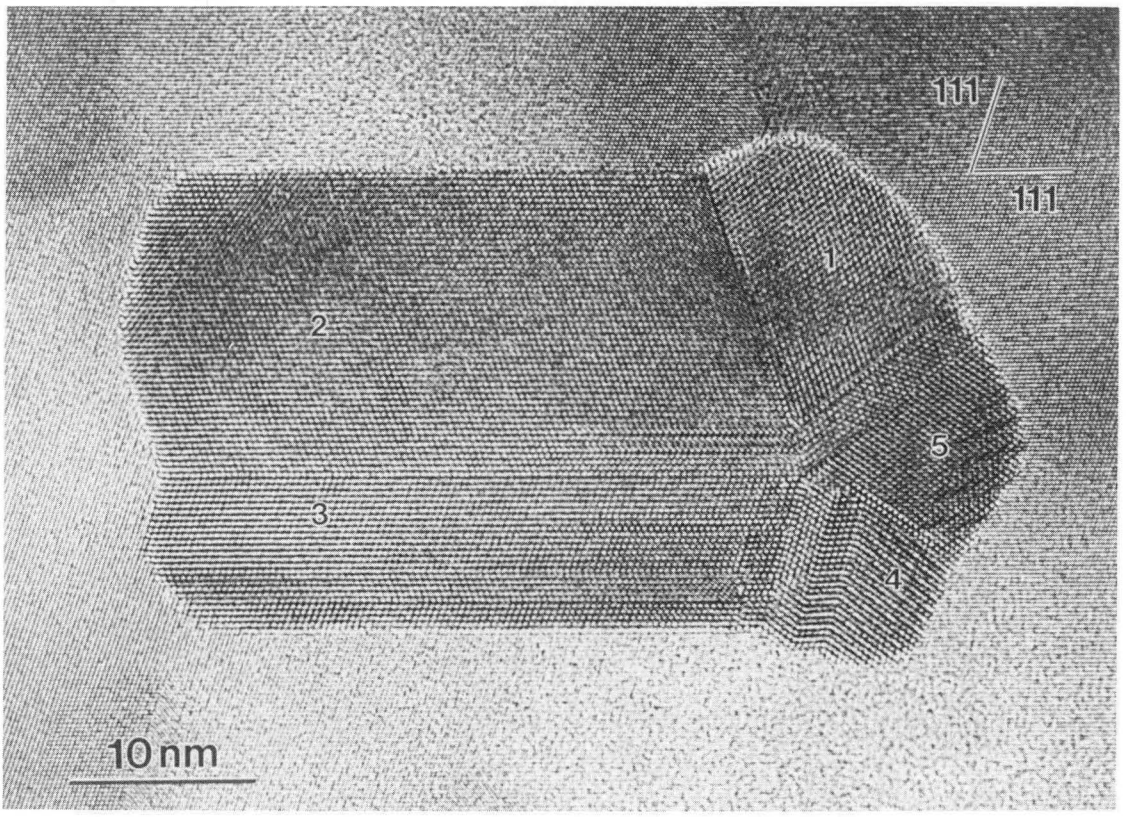

XBB 894-3217

FIGURE 11

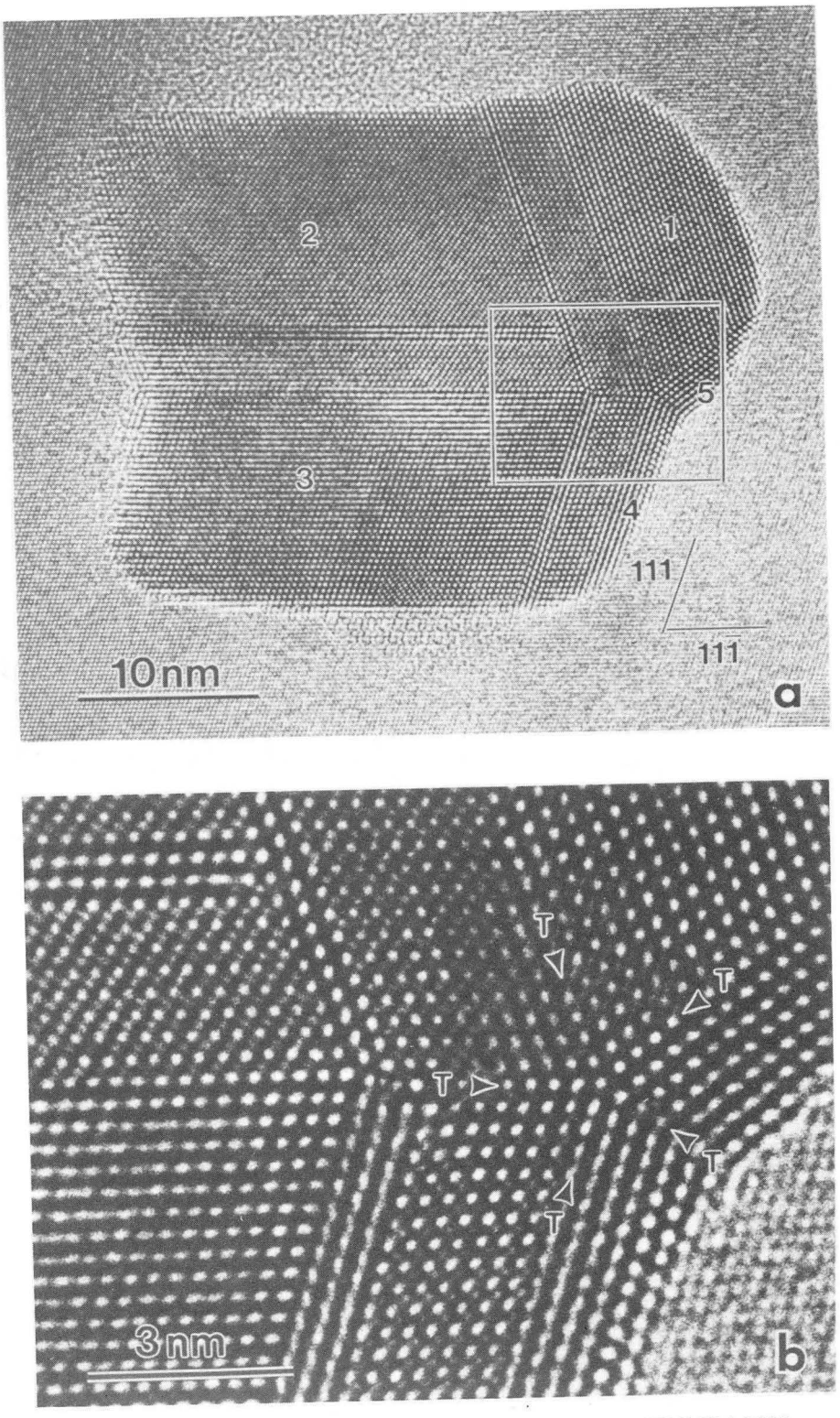

XBB 894-3220

FIGURE 12

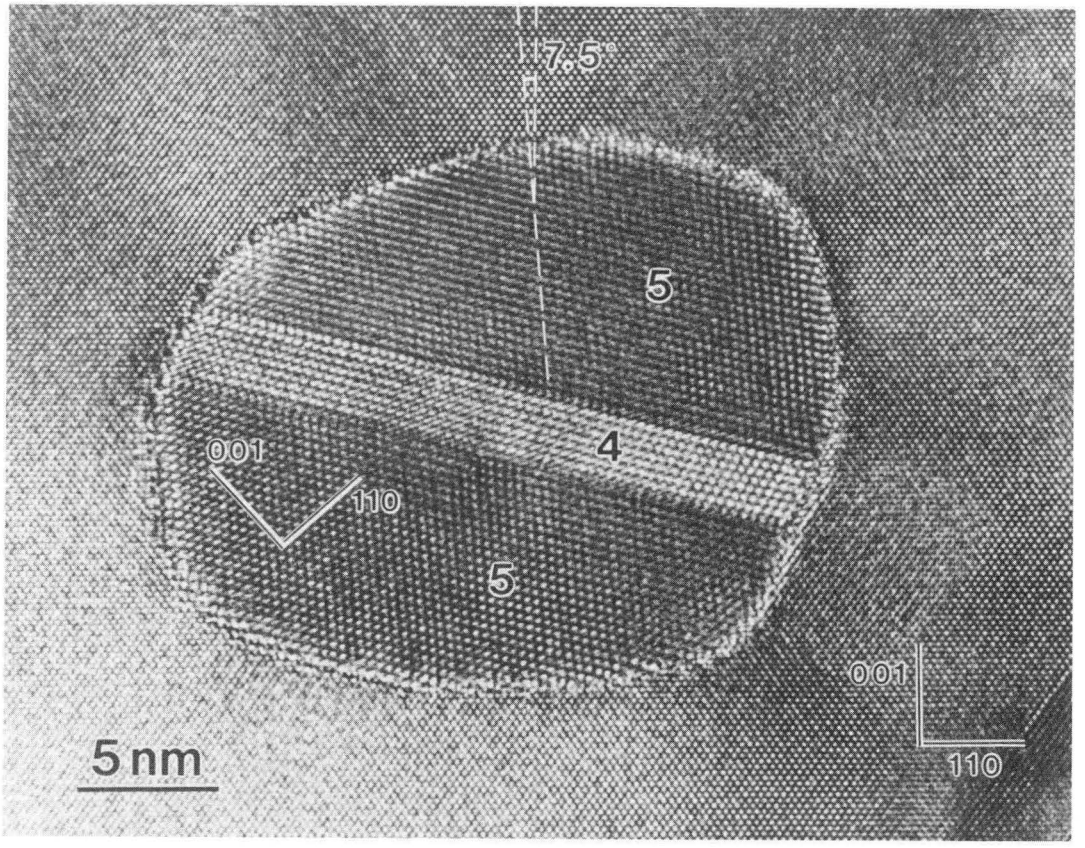

XBB 894-3219

FIGURE 13a

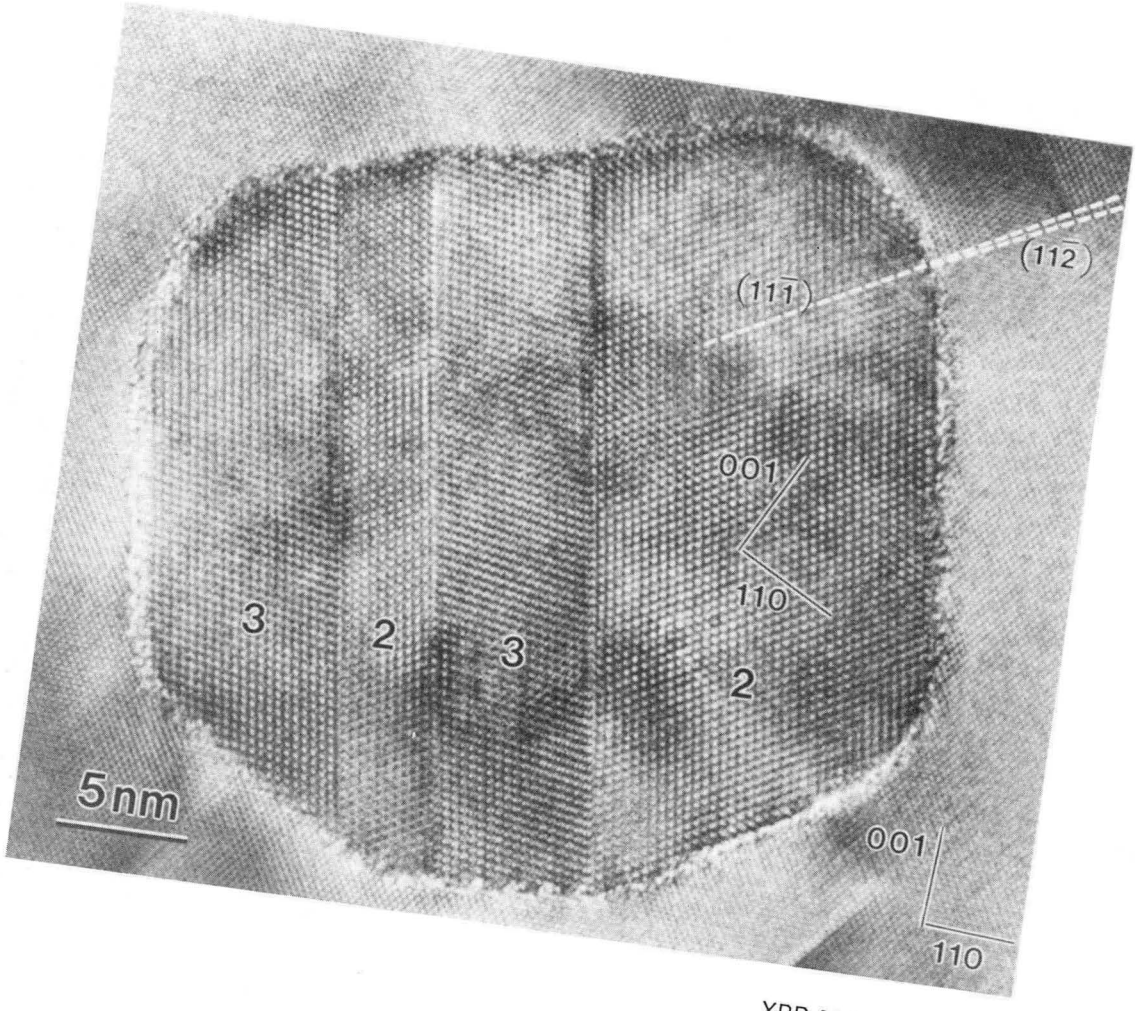

XBB 894-3218

FIGURE 13b

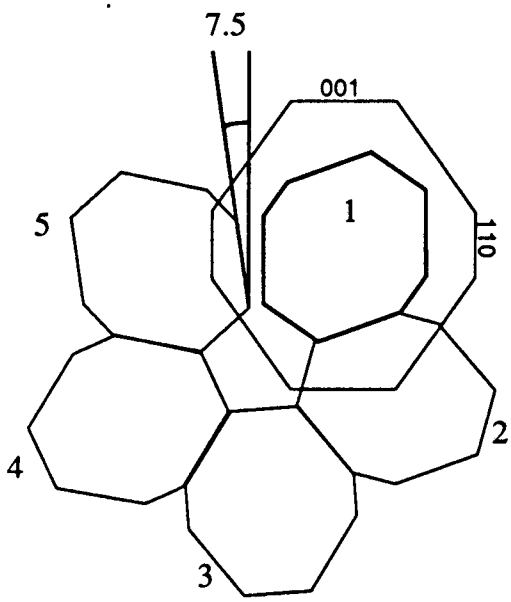

c)

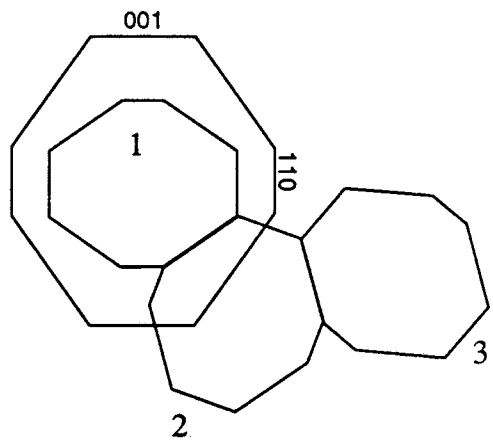

d)

XBL 894-1477

Figure 13

a)

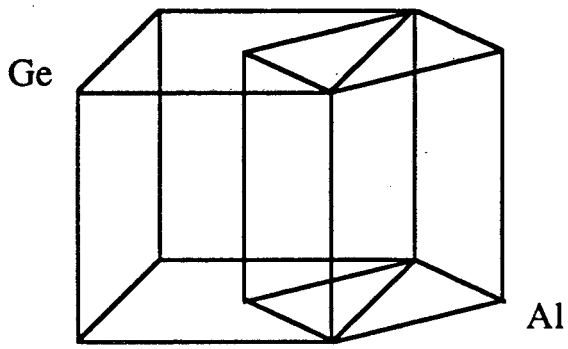

b)

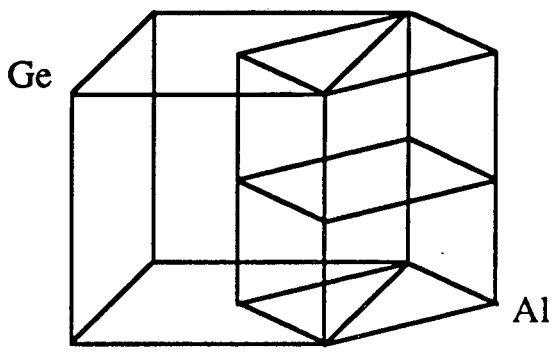

XBL 901-270

Figure 14

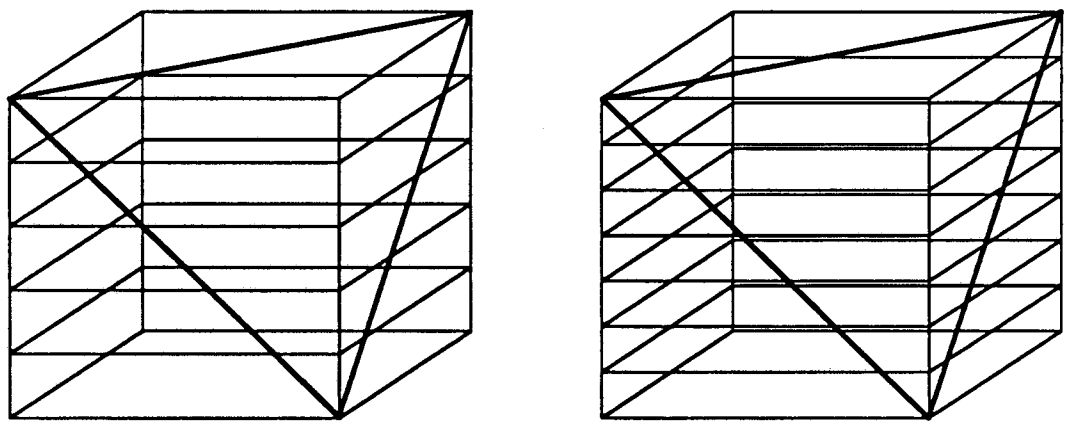

Ge Al

near-CSL 125 / 343

XBL 901-271

Figure 15

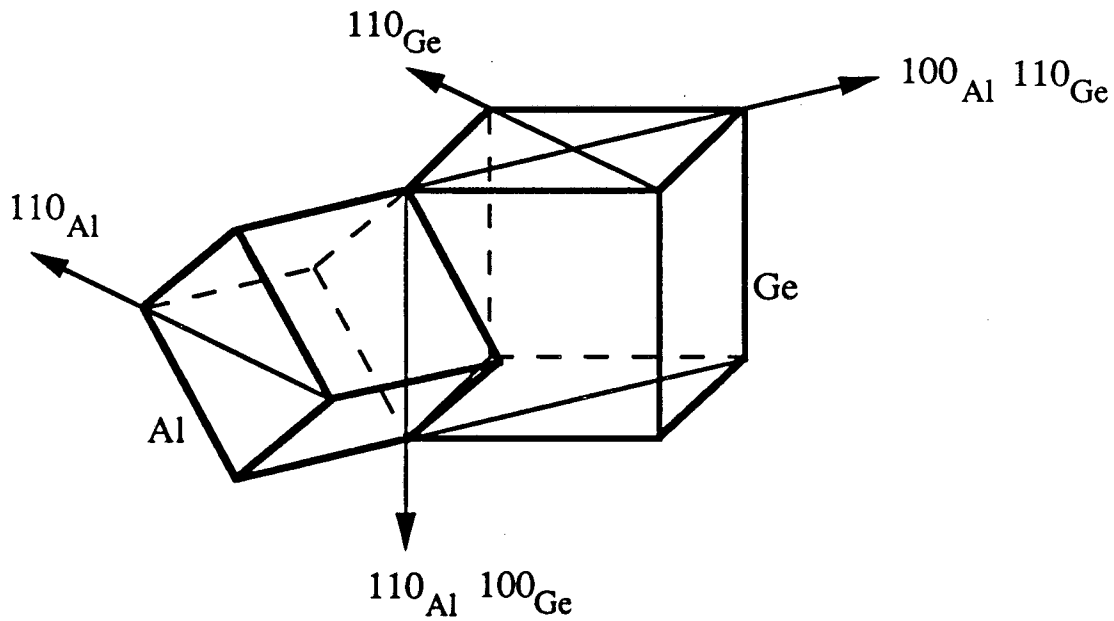

XBL 901-276

Figure16

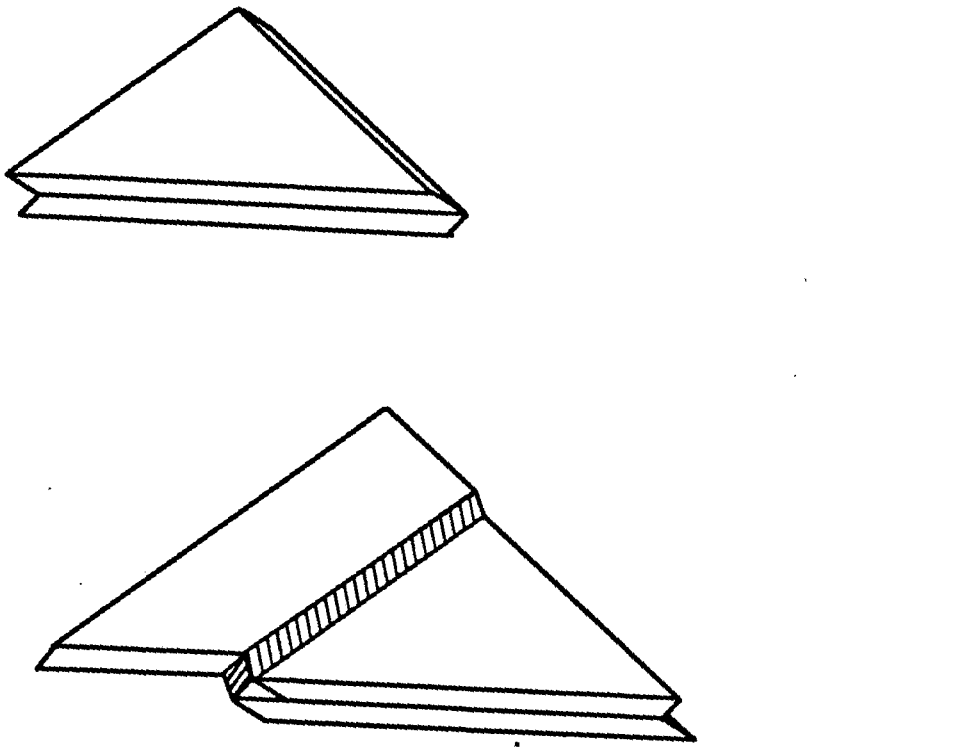

Figure 17

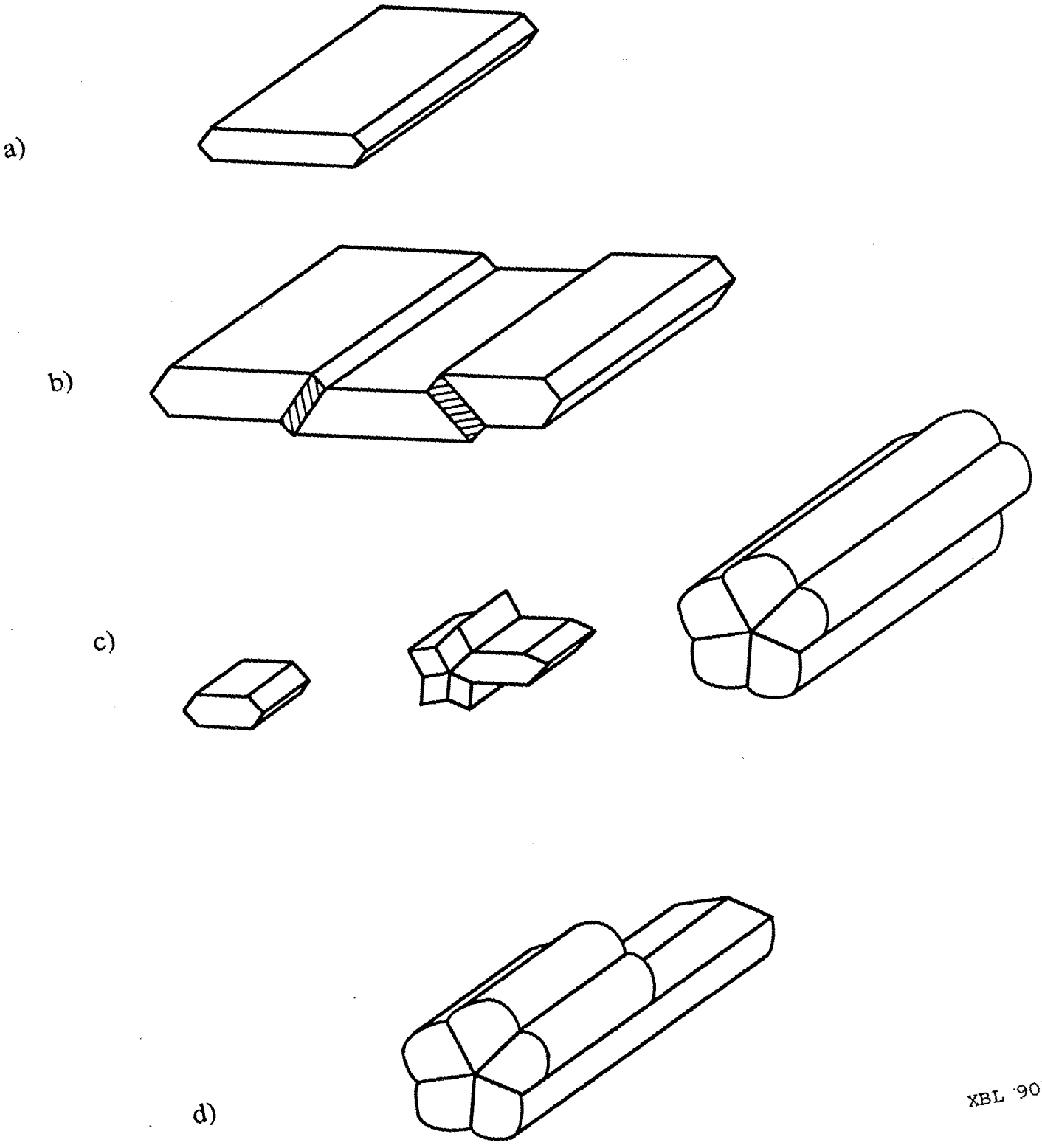

Figure 18

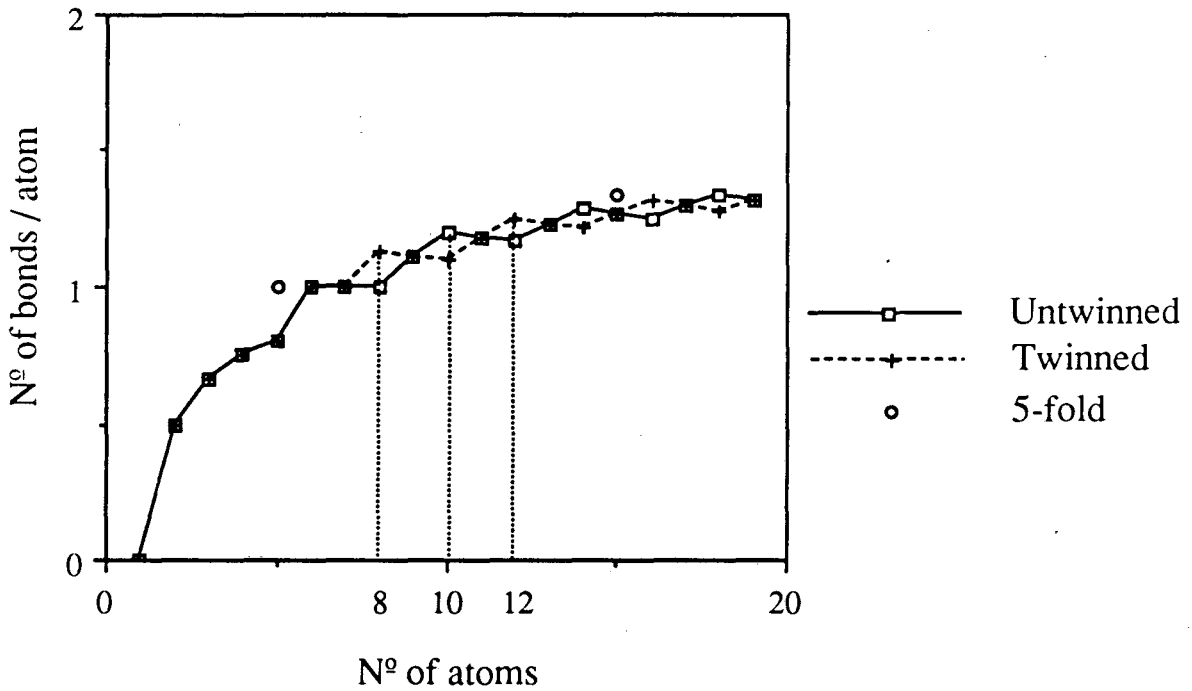

XBL 894-1478

Figure 19

a)

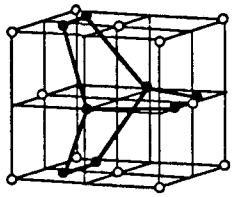

Twinned
8 Ge

b)

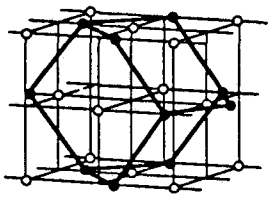

Untwinned
10 Ge

○ Al
● Ge

c)

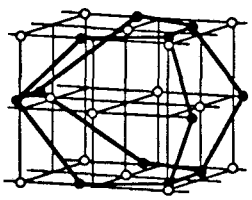

Twinned
12 Ge

d)

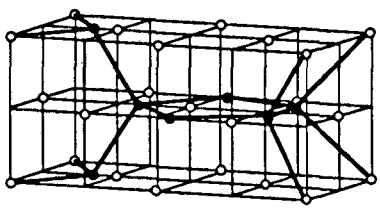

e)

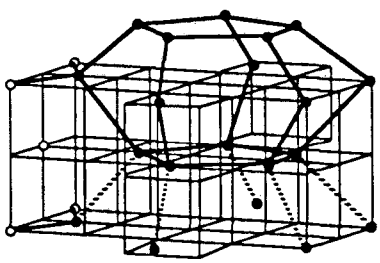

Five-fold
15 Ge

XBL 894-1479

Figure 20

a

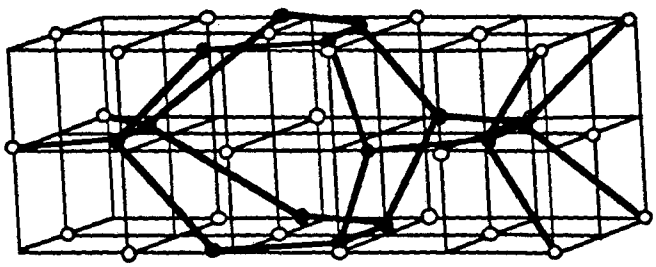

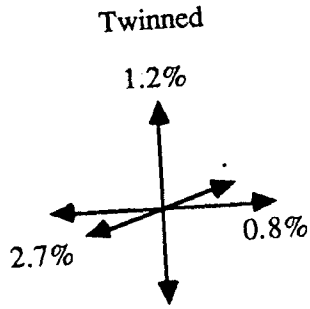

b

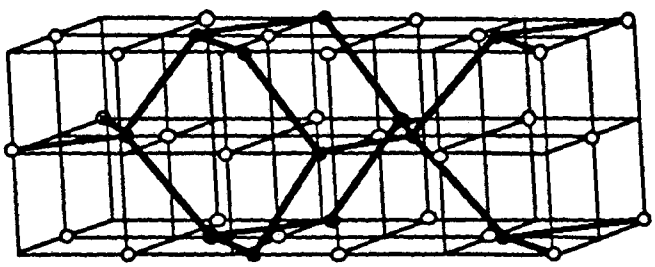

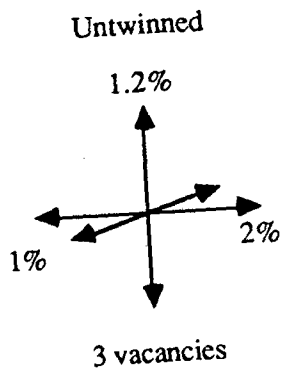

XBL 894-1480

Figure 21

LAWRENCE BERKELEY LABORATORY
TECHNICAL INFORMATION DEPARTMENT
1 CYCLOTRON ROAD
BERKELEY, CALIFORNIA 94720